Femtosecond Time-Resolved Studies on the Reaction Pathways for the Generation of Reactive Oxygen Species in Photodynamic Therapy by Indocyanine Green

by

Ting Luo

A thesis
presented to the University of Waterloo
in fulfillment of the
thesis requirement for the degree of
Master of Science
in
Physics

Waterloo, Ontario, Canada, 2008

I hereby declare that I am the sole author of this thesis. This is a true copy of the thesis, including any required final revisions, as accepted by my examiners.

I understand that my thesis may be made electronically available to the public.

Abstract

Photodynamic therapy (PDT), which utilizes the combination of light and a photosensitizing drug to cause tissue damages, has emerged as a novel clinical approach for the treatment of numerous cancers, as well as some other non-malignant conditions. Although a few photosensitizers have been approved for clinical uses, the mechanism of drug action, especially the initial photochemical reactions that lead to the formation of the reactive oxygen species (ROS), is still not well understood. Moreover, the PDT efficiency of currently used drugs is limited due to the strong attenuation of light by tissues in the wavelength range of 630-690 nm, where these drugs are photo-activated. Photosensitizers which are sensitive to near infrared (NIR) light are believed to be able to overcome this limitation.

In this thesis work, the molecular mechanism of action of indocyanine green (ICG), a potential NIR PDT drug, was investigated using our femtosecond time-resolved laser spectroscopy. Femtosecond time-resolved fluorescence decay profiles of ICG in water were obtained using the fluorescence up-conversion technique. The lifetime of ICG excited singlet state was determined to be about 150 ps, directly from the fluorescence decay kinetic traces. The excited triplet-state yield of ICG in water was found to be extremely low, according to the result of the ground-state bleaching recovery measurement. This observation is contrary to the conventional understanding that the ROS would be generated mainly from the excited triplet state of the photosensitizer and, therefore, suggests the existence of a new reaction pathway. Pump-probe transient absorption spectroscopy was applied to study the reaction between ICG and oxygen in more details. The results reveal that the formation of ICG and oxygen ground-state complexes ($[ICG]_m$:$[O_2]_n$) is a key step in the generation of the ROS. Electron transfer from the excited singlet state of ICG to oxygen has been proposed to be a possible pathway for the generation of ROS.

Acknowledgements

I would like to thank my supervisor Prof. Qing-Bin Lu and co-supervisor Prof. Donna Strickland, for their guidance and support during the past two years. I would also like to thank Prof. Bae-Yeun Ha and Prof. Hartwig Peemoeller for their time and comments. Many thanks go to all the other members of Prof. Lu's laboratory, for their support and friendship.

To my family

Contents

List of Figures

List of Tables

Chapter 1

Introduction

Cancer is a leading cause of human death. It can be treated by surgery, chemotherapy, radiotherapy, or other methods. Photodynamic therapy (PDT), which involves the administration of photosensitizing drugs and subsequent exposure of the tissue to light, has emerged as a novel clinical approach for the treatment of various tumors and some other non-malignant conditions [1, 2]. Due to the selectivity of drug uptake [3] and the control of light delivery, PDT has the potential of inducing effective cytotoxicity in malignant tissue and limited damage to the surrounding healthy tissues. Therefore, PDT has superior properties compared with conventional cancer therapies such as chemotherapy and radiotherapy: it is selective, noninvasive, and has few side effects. Over the past 30 years, PDT has been successfully applied for the treatment of a variety types of cancers, such as early lung cancers not suitable for resection [4, 5], brain tumors [6, 7], head and neck lesions [8, 9], and rectal cancer [10]. A few PDT sensitizers have been approved for clinical uses.

The therapeutic effect of PDT is generally believed to be mainly from the reactive oxygen species (ROS) generated by the reaction of the excited photosensitizer molecules with oxygen. At the cellular and tissue levels, the ROS can cause cellular or vascular damages and have immunological effects [11]. However, at the molecular level, the mechanisms for drug action, especially the very initial photochemical reactions leading to the generation of the ROS, have only been poorly understood. Moreover, the efficiency of currently used PDT drugs is limited by the light penetration depth in tissue, since the

absorption of these drugs lies in the visible light wavelength range (400 to 700 nm), where the attenuation of light by tissue is strong [12].

One of the current research focuses is to develop new photosensitizers that are sensitive to near-infrared (NIR) light. Indocyanine green (ICG), which has a strong absorption band in the range of human tissue optical window [12], is a potential NIR PDT sensitizer. In this thesis, real-time studies of the reaction mechanisms of ICG in water have been performed using high-sensitivity femtosecond time-resolved laser spectroscopy. A new reaction pathway for the generation of ROS has been proposed. This study thus provides new insight into the molecular mechanism for the formation of ROS in PDT.

1.1 Cancer and Cancer Treatment

Cancer is a disease characterized by uncontrolled cell growth and division, invasion and sometimes metastasis (the spread of cancer cells from their primary site to a remote organ). The process of cancer development may take years before clinical signs are evident. This is a multistage process with accumulation of "permanent new characters" [13] as a result of exposure to carcinogens, which refer to harmful molecules or conditions originating from within or outside the body. The most common examples of carcinogens are:

- chemicals such as benzene, kepone,and asbstos,
- microbial carcinogens such as aflatoxin B1,
- viruses such as Hepatitis B and human papilloma viruses,
- sources of ionizing radiation such as radon gas.

In most cases, cancers are sporadic (that is, not inherited). But a few syndromes have been found to be hereditable. For example, inherited mutations in the genes BRCA1 (breast cancer 1) and BRCA2 (breast cancer 2) are associated with an elevated risk of breast cancer [14, 15] and ovarian cancer [16]; hereditary nonpolyposis colorectal cancer (HNPCC, also known as Lynch syndrome) can include familial cases of colon cancer,

uterine cancer, gastric cancer, and ovarian cancer, without a preponderance of colon polyps [17]; retinoblastoma, when occurring in young children, is due to a hereditary mutation in the retinoblastoma gene [18].

Currently, there are a number of therapies available for the treatment of cancers, such as surgery, chemotherapy, radiotherapy, immunotherapy, monoclonal antibody therapy, or a combination of these approaches. The choice of therapy is mainly based on the type and stage of the disease, as well as the general condition of the patient.

1.1.1 Surgery

Surgery is the most frequently used approach for the treatment of solid tumors via the removal of either the tumor or the entire organ. It is often combined with other cancer treatments, such as chemotherapy and radiotherapy, depending on the type and stage of the cancer. Surgery is also necessary in order to determine the type, stage, and extent of spread of tumors.

In principle, if entirely removed, solid tumors can be cured by surgery. However, in practice, a single cancer cell is invisible to the naked eye but can regrow into a new tumor (recurrence). When the cancer cell has metastasized to other sites prior to surgery, complete excision is impossible.

Side effects including anesthesia complications, infections, and immune suppression also exist after surgical removal of tumors. Sometimes, the removal of the primary tumor may even stimulate cancer metastasis [19, 20], which is associated with poorer survival. Moreover, the reason why the spread begins rapidly following surgery is still not fully understood.

1.1.2 Radiotherapy

Ionizing radiation is used in radiotherapy to damage or kill cancer cells by damaging their genetic material, making it impossible for these cells to continue to grow and divide. Although radiation damages both cancerous and normal cells, most normal cells can

recover and function properly. Thus, it is usually given in fractions, which allows the healthy tissue to recover at the intervals. As a result, the effects of radiation therapy are localized.

Radiotherapy may be applied pre-operatively to shrink the tumor in order to facilitate surgery, or given postoperatively as adjuvant therapy to reduce the probability of local recurrence. Almost every type of solid tumor and some leukemia and lymphoma can be treated by radiotherapy.

Radiotherapy does have potential disadvantages. Despite huge improvements achieved in reducing severe side effects such as skin burns and scarring, side effects such as tiredness, local skin changes (itching, tenderness, swelling or soreness), nausea, and vomiting may continue for a few weeks. Moreover, the therapeutic efficiency of radiotherapy for solid tumors with hypoxic regions is limited due to resistance of hypoxic cells to ionizing radiation [21].

1.1.3 Chemotherapy

Chemotherapy is the treatment of cancer via application of anticancer drugs which can destroy cancer cells or inhibit their growth. Unlike surgery or radiotherapy, chemotherapy is systemic. Its selectivity mainly relies on the selective uptake of the drug molecules by the cancer cells. In general, chemotherapy affects rapidly dividing cells; chemotherapy drugs may interfere with cell division in various ways, for example with the duplication of DNA or the separation of newly formed chromosomes.

Pre-operative chemotherapy may be used to reduce the size of the tumor, to facilitate complete surgical excision, while adjuvant chemotherapy is applied to decrease the rate of relapse or improve survival after surgery or radiotherapy treatment. Chemotherapy is also used to relieve symptoms and prolong life when a cure is not possible.

Chemotherapy has the potential of damaging healthy tissues, especially those with a high replacement rate (e.g. the intestinal lining), since it targets all rapidly dividing cells without specificity. Numerous side effects can thus occur following treatment. These include pain, diarrhea, constipation, mouth sores, hair loss, nausea and vomiting, as

well as blood-related side effects. Another drawback of chemotherapy comes from the occurrence of drug resistance. Often, if a cancer becomes resistant to one drug, it is more likely to be resistant to other drugs [22]. Therefore, it is especially important to choose the best possible treatment protocol.

By using surgery or radiotherapy, localized cancers can usually be effectively treated, but more than 50% of the cancers have already metastasized when diagnosed [23]. Chemotherapy can be used to kill cancer cells throughout the body. Unfortunately, currently available chemotherapy drugs are not specific for cancer cells; they generally attack all dividing cells and, therefore, have strong side effects. In recent years, much progress have been made in cancer diagnosis and treatment. Various targeted therapies are being developed in an attempt to attack specific targets involved in carcinogenesis and tumor growth such as HER2 (human epidermal growth factor receptor 2) [24] and VEGF (vascular endothelial growth factor) [25]. Several compounds have shown promise in the management of various cancers [26].

In summary, although significant advances have been made over the past decades, the survival rate of cancer patients, unless detected in the early stage, is still very low. More effective cancer treatment strategies and new drugs are still urgently needed. A better understanding of drug action mechanisms may facilitate the process of drug discovery [27].

1.2 Photodynamic Therapy

Cell death induced by the interaction of light and chemicals was first reported more than one hundred years ago by a German medical student named Oscar Raab [28]. The medical application of photodynamic therapy (PDT) was first described in 1903 by von Tappeiner and Jesionek, who used the combination of light and topically applied eosin to treat basal cell carcinomas (BCCs) [29]. However, little study was performed on the clinical applications of PDT until 69 years later; Diamond *et al.* [30] proposed that the combination of tumor-localizing and phototoxic properties of porphyrins might be exploited for the treatment of cancer. Later in 1975, Dougherty and coworkers [3] reported the first case of successful treatment of experimental animal tumors by PDT. In the same

year, Kelly showed that PDT treatment could destroy human bladder tumor cells transplanted into mice [31]. Three year later, Dougherty reported the first successful treatment of a large series of patients with PDT [32]. Since then, a large number of studies have been published in support of the clinical effectiveness of PDT for the treatment of various cancers.

1.2.1 Conventional Mechanism of PDT

Figure 1.1 illustrates some of the processes that can occur after a molecule absorbs a photon with appropriate energy. The first step is the promotion of the molecule from its ground electronic state (S_0) to an excited singlet state, usually S_1. According to Frank-Condon principle, the time of an electronic transition (on the order of 10^{-15} s) is much shorter than that of neclear rearrangement (on the order of 10^{-13} to 10^{-14} s) [33]. As a result, this electronic transition occurs without causing any significant displacement of the nuclei. If the molecule is promoted to a higher excited singlet state (e.g. S_2), it will undergo a fast internal conversion (IC) to a vibrationally-excited state of S_1 (S_1^v). This process is followed by a rapid vibrational relaxation (VR), in which S_1^v loses its excess energy through collision with solvent molecules. From the lowest, zero-point vibration level of S_1 state (S_1^0), the molecule can go back to its ground state via either radiation emission (fluorescence) or internal conversion. A crossing from S_1^0 to the excited triplet state (T_1^v) can also take place through another radiationless process, called intersystem crossing (ISC). A radiative transition known as phosphorescence can bring the molecule from T_1^0 back to the ground state.

The lifetime of the excited triplet state is typically tens of microseconds due to the spin-forbidden nature of the T_1-S_0 transition [34]. In PDT, it is generally believed that the long lifetime of the excited triplet state allows sufficient time for the photosensitizer to interact with surrounding molecules to produce cytotoxic species. Therefore, the quenching of the excited triplet state of the photosensitizer ($^3P^*$) is considered to be the major process to induce photodynamic damages. There are two proposed mechanisms for the reaction of the $^3P^*$ with bio-molecules, known as the type I and type II reactions (Figure 1.2) [11, 34–36].

In a type I process, the photosensitizer reacts with solvent or a substrate molecule

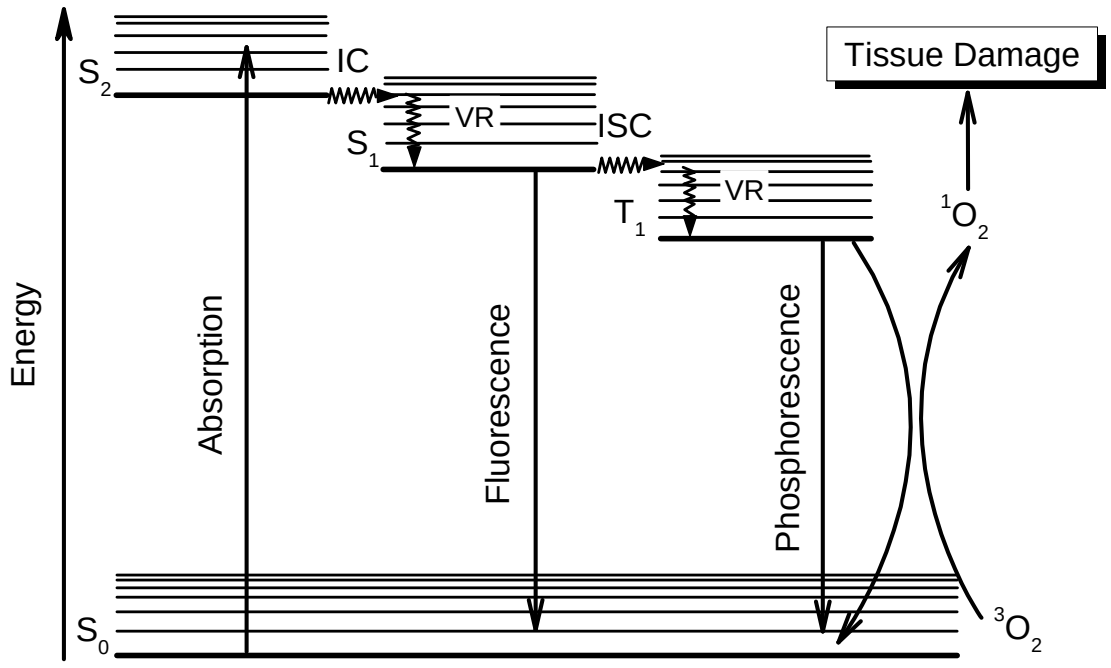

Figure 1.1: Jablonski diagram showing the possible fates of a PDT drug molecule following photo-excitation. S_0 is the ground electronic state of the molecule. S_1 and S_2 are the excited singlet states. T_1 is the lowest excited triplet state. (IC: internal conversion; VR: vibrational relaxation; ISC: intersystem crossing.)

by electron/hydrogen transfer to produce highly reactive free radicals. Figure 1.2 shows the reaction with water to generate the hydroxyl radical ($^{\cdot}OH$) and hydrogen peroxide (H_2O_2). A type II reaction, however, produces an electronically excited state of oxygen known as the singlet oxygen ($^1O_2$) through energy transfer.

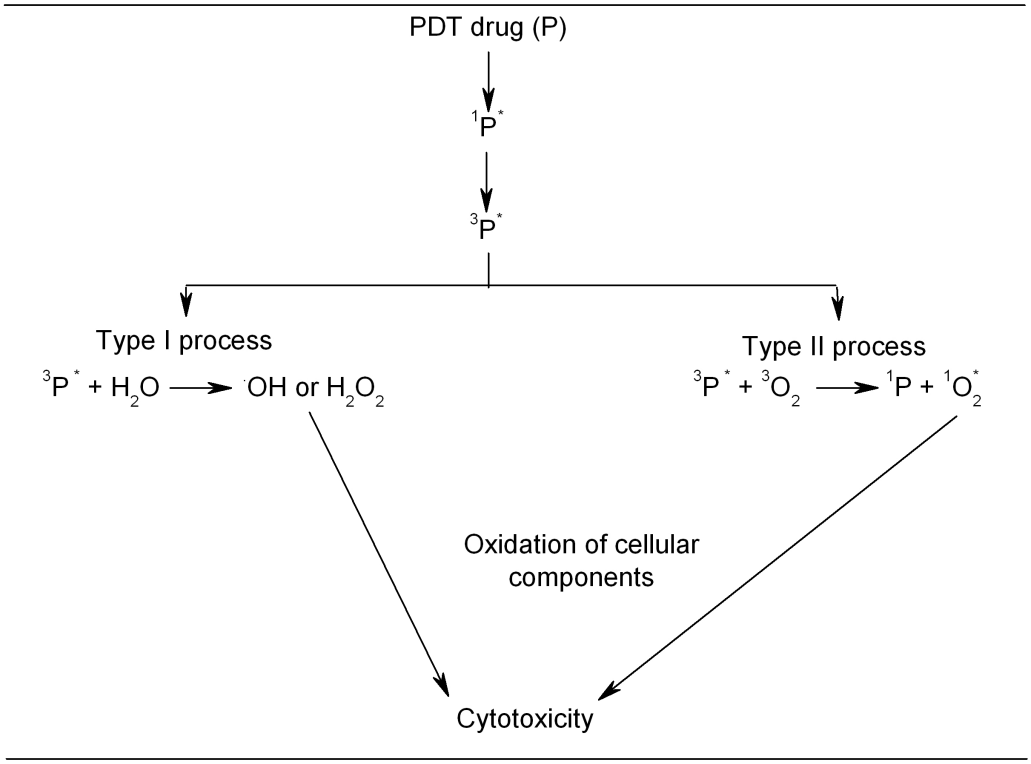

Figure 1.2: Mechanism of photodynamic photooxidation, adopted from Ref. [11].

At the cellular and tissue levels, the reactive oxygen species (ROS) such as $^{\cdot}OH$, H_2O_2, and $^1O_2$ generated in PDT can cause tumor destruction by direct killing of tumor cells, damaging the tumor vasculature, or activating an immune response against tumor growth [37]. Both type I and II processes contribute to the production of ROS and their contribution depends on the photosensitizing drug used, drug concentration and oxygen tension [38]. However, it is generally believed that the $^1O_2$ is the most important ROS generated in PDT [39, 40] and the type II process is the main pathway.

1.2.2 Singlet Oxygen

Molecular oxygen is one of the most important substances on the earth; it is involved in all living processes. To a great extent, the special nature of oxygen comes from the existence of two low lying excited singlet states, namely $^1\Delta_g$ and $^1\Sigma_g^+$. Figure 1.3 shows the electron occupancy of these two states. In condensed media, the higher energy state $^1\Sigma_g^+$ is rapidly converted to $^1\Delta_g$ (i.e. the singlet oxygen).

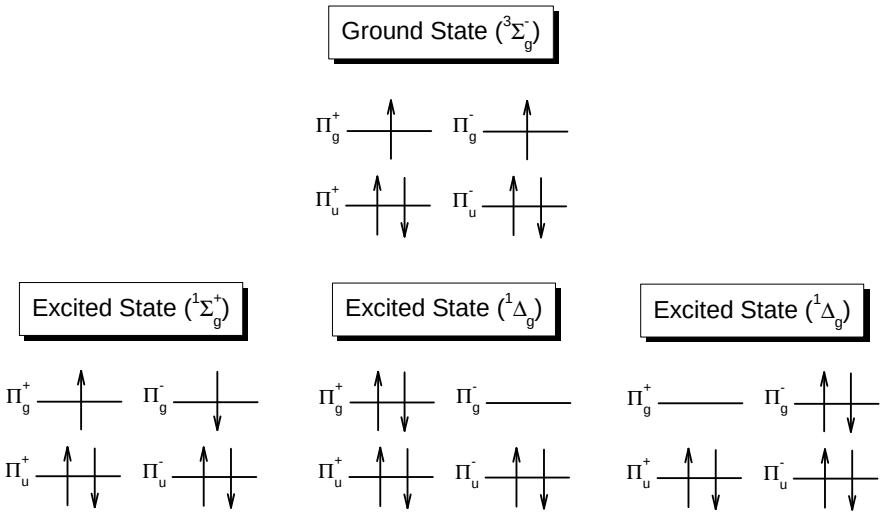

Figure 1.3: Electron occupation of molecular orbitals in oxygen.

Since $^1O_2$ has a long lifetime and a low energy level ($^1\Delta_g \rightarrow ^3\Sigma_g^-, \tau = 45$ min, $\nu_{00} = 7882.39$ cm^{-1} [41]), it is the active species in many important photoprocesses [42]. It can react directly with various types of organic compounds with double bonds. Most of the reactions fall into the following three classes.

Ene reaction:

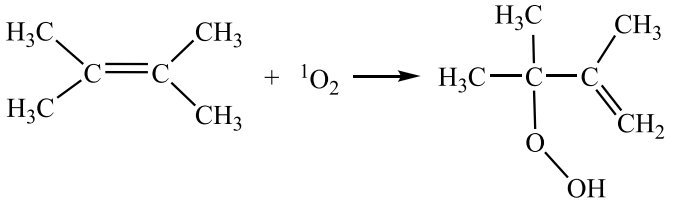

1,2-Cycloaddition:

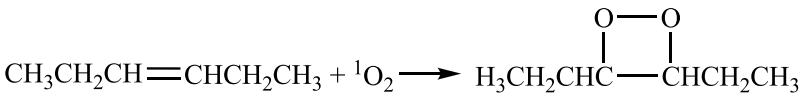

1,4-Cycloaddition:

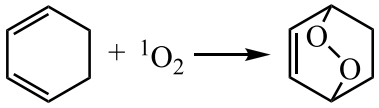

Biological membranes are the key targets for photomodification in tumor cells following PDT treatment [43–46]. Virtually all components of cell membranes including phospholipids, proteins and cholesterol are readily oxidized by $^1O_2$. Unsaturated lipids can be oxidized. The products can then break down to free radicals and initiate chain oxidation of other unsaturated lipids. In membrane proteins, tyrosine, tryptophan, histidine, methionine, and cysteine are vulnerable [47] and the protein peroxides can also decompose to generate free radicals. Oxidation of cholesterol by $^1O_2$ produces cholesterol 5α-hydroperoxide [48].

A key property of a photosensitizer is the quantum yield of singlet oxygen (Φ_Δ) which is defined as:

$$\Phi_\Delta = \frac{\text{The number of } {}^1O_2 \text{ generated}}{\text{The number of photons absorbed}} \tag{1.1}$$

In practice, measurements of Φ_Δ are usually scaled to standard references such as rose bengal, which has a Φ_Δ of 0.76 in aqueous media [49].

There are three techniques frequently used for the detection and measurement of singlet oxygen.

Singlet oxygen phosphorescence at 1270 nm: This is a gold standard for $^1O_2$ identification. In the flash photolysis technique, the sample is irradiated with a strong light flash. The height of the luminescence pulse is proportional to the yield of $^1O_2$ and the decay corresponds to the lifetime. The lifetime is highly dependent on the medium. Another test for $^1O_2$ is based on the fact that solvent deuteration gives rise to an increase in the lifetime of more than an order of magnitude [50].

Protective effects of additives: Indirect methods for $^1O_2$ identification are based on the inhibiting effects of an additive on the rate of a photochemical reaction. Azide ion (N_3^G) is a useful water-soluble agent. The protective effect of azide is attributed to physical quenching. Other frequently used water-soluble quenchers include 1,4-diazabicyclo-[2.2.2]octane (DABCO), ascorbic acid, and tryptophan. Some $^1O_2$ quenchers used in organic solvents and phospholipid membranes include cholesterol, -tocopherol and -carotene.

Electron paramagnetic resonance or electron spin resonance: Singlet oxygen is a non-magnetic molecule and cannot be detected directly by EPR. However, the reaction of $^1O_2$ with a stable molecule such as 2,2,6,6-tetramethyl-4-piperidone (TEMP) can generate a moderately long-lived free radical whose structure as determined by EPR provides an unambiguous identification.

1.2.3 Photosensitizers

The photosensitizer is a critical element in PDT. For the treatment of cancer, an ideal photosensitizer should meet the following requirements:

- Have the ability to selectively accumulate in the cancerous tissues.
- Have minimum dark toxicity and be cytotoxic in the presence of light.
- Absorb significantly in the tissue optical window [12].
- Have a high quantum yield and long lifetime of triplet state.
- Be rapidly excreted from the body.

More than a century ago, eosin was first used as a photosensitizer to treat epilepsy [51] and skin tumors [29]. However, the lack of suitable sensitizers and light sources made it impossible to use PDT clinically at that time. The situation changed in the 1970s when the ferric ion-free derivative of haem (haematoporphyrin derivative, HpD) and its purified form porfimer sodium (Photofrin®) became available. The first large series of successful HpD-mediated PDT treatment in humans were reported by Dougherty *et al.*

in 1978. All tumors treated were found to be responsive [32]. Photofrin® was approved by the U.S. Food and Drug Administration (FDA) in 1995 and has been approved in several other counties including Canada, Netherlands, Japan, France, and Italy or the treatment of specific tumors [52]. However, the use of the "first-generation photosensitizers", including HpD and its commercial variants Photofrin®, Photosan®, Photogem®, and Photocarcinorin®, is limited to selected tumors due to two important disadvantages. Firstly, they have the potential of developing severe, prolonged and generalized phototoxic reactions in the skin following PDT. Secondly, they are in complex and variable mixtures forms and have not proved possible to isolate a single active component.

Table 1.1: Photosensitizers that have been approved for clinical uses

Photosensitizer	Type of disease	Country
Photofrin®	Barrett's HGD	Canada, EU, UK, USA
	Cervical dysplasia	Japan
	Cervical cancer	Japan
	Endobronchial cancer	Canada, Denmark, Finland, France, Germany, Ireland, Japan, The Netherlands, UK, USA
	Esophageal cancer	Canada, Denmark, Finland, France, Ireland, Japan, The Netherlands, UK, USA
	Gastric cancer	Japan
	Papillary bladder cancer	Canada
ALA (Levalan®, Metvix®)	Actinic keratosis	EU, USA
ALA (Metvix®)	Basal cell carcinoma	EU
Foscan®	Head and neck cancer	EU, Norway, Iceland

ALA: 5-aminolevulinic acid; EU: European Union; HGD: high-grade dysplasia; UK: United Kingdom; USA: The United States.

Many new compounds have been synthesized in an attempt to create PDT agents better than Photofrin®. In 1990s, several "second-generation photosensitizers", including 5-aminolaevulinic acid (ALA) and its methyl ester (methyl aminolaevulinate, MAL), benzoporphyrin derivatives, phthalocyanines, chlorins and porphycenes were developed. These synthetic dyes are chemically pure, highly efficient, selective and safe. In addition, the skin photosensitivity of these compounds lasts for only a short time. ALA

(Levulan®) was approved in 1999 for the treatment of cancerous lesions. The methyl ester of ALA (Metivx®) was approved in 2001 for the treatmend of BCC and actinic keratosis. In the same year, mTHPC (temoporfin, Foscan®) was approved for the treatment of head and neck cancer. Table 1.1 is a list of the photosensitizers that have been approved for clinical uses [38, 53].

1.2.4 Indocyanine Green as a Potential Near Infrared Photosensitizer

The clinic effectiveness of PDT also depends on the wavelength of the light source used. Light penetration into tissue is limited by light scattering and absorption. The penetration depth of light in tissue as a function of wavelength has been measured by Eichler *et al.* [12]. According to this report, the light penetration depth in tissue between 630 and 690 nm, where most of the currently used photosensitizers are activated, is on the order of 1-2 mm [12]. However, the attenuation of light by tissue is much weaker in the wavelength range from $\sim$700 nm to $\sim$930 nm (the tissue optical window, as shown in Figure 1.4) [54]. Therefore, one of the approaches to improve PDT efficiency is to develop new photosensitizers that are sensitive to near infrared (NIR) light.

The dye indocyanine green (ICG, Figure 1.5(a)) was approved by the U.S. FDA in 1956. Since then, it has been widely used in medical diagnosis for blood volume determination [55], choroidal angiography [56, 57], cardiac output measurement [58], fluorescence probing of proteins [59], and pharmacokinetic analysis [60]. It has also been considered to be a potential NIR PDT sensitizer. The static absorption spectrum of ICG (Figure 1.5(b)) shows that it has an absorption maximum of 778 nm in pure water. When ICG is dissolved in plasma, the absorption peak is shifted to 805 nm [61], falling into the wavelength range of the human tissue optical window [12].

Potential applications of ICG in PDT have been reported by several groups [62–65]. Indocyanine green-induced photo-oxidative killing of human cancer cells has been reported and the involvement of singlet oxygen has been suggested on the basis of the inhibition effect of the singlet oxygen quencher sodium azide on cell killing [63, 65]. However, direct detection of singlet oxygen luminescence at 1270 nm was unsuccessful

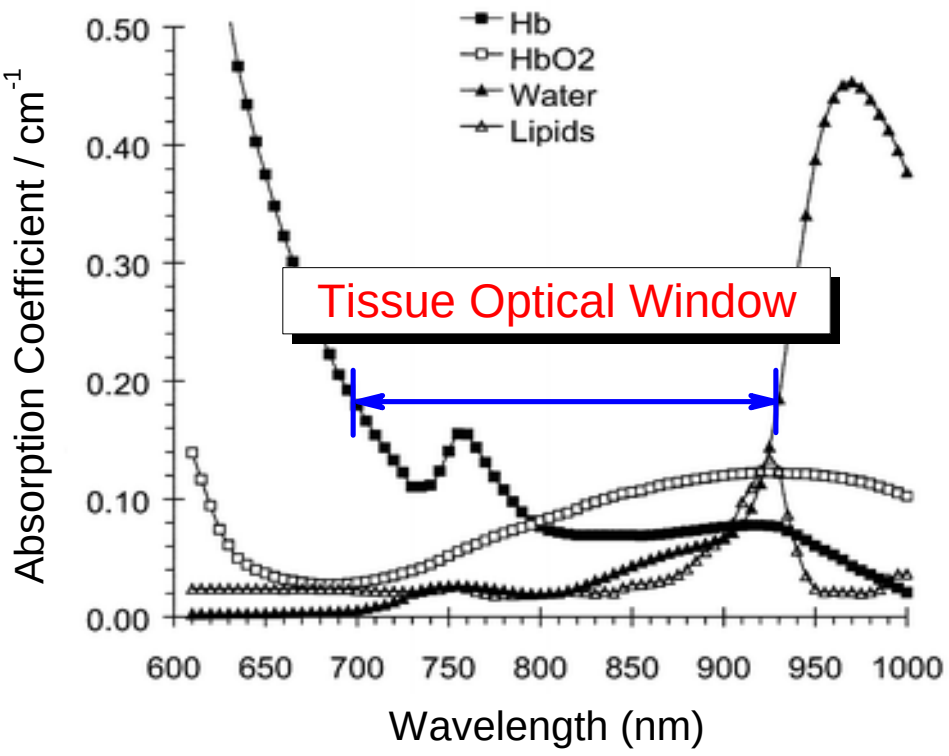

Figure 1.4: Light absorption by four main tissue components: deoxyhaemoglobin (Hb), oxy-haemoglobin (HbO_2), water, and lipids, in the spectral range of 600-1000 nm. The wavelength range of ∼700 to ∼930 nm is known as the tissue optical window, where the attenuation of light by tissue is much weaker than that in the other wavelength ranges. This figure is adapted from [54].

[66]. Moreover, the triplet quantum yield of ICG was found to be extremely low [67, 68]. Therefore, it is still an open question wether the ROS would be generated via the conventional mechanism of PDT which involves the long-lived excited triplet state of the sensitizer. The exact mechanism of drug action, especially the initial photochemical reaction leading to the formation ROS, is still not well identified.

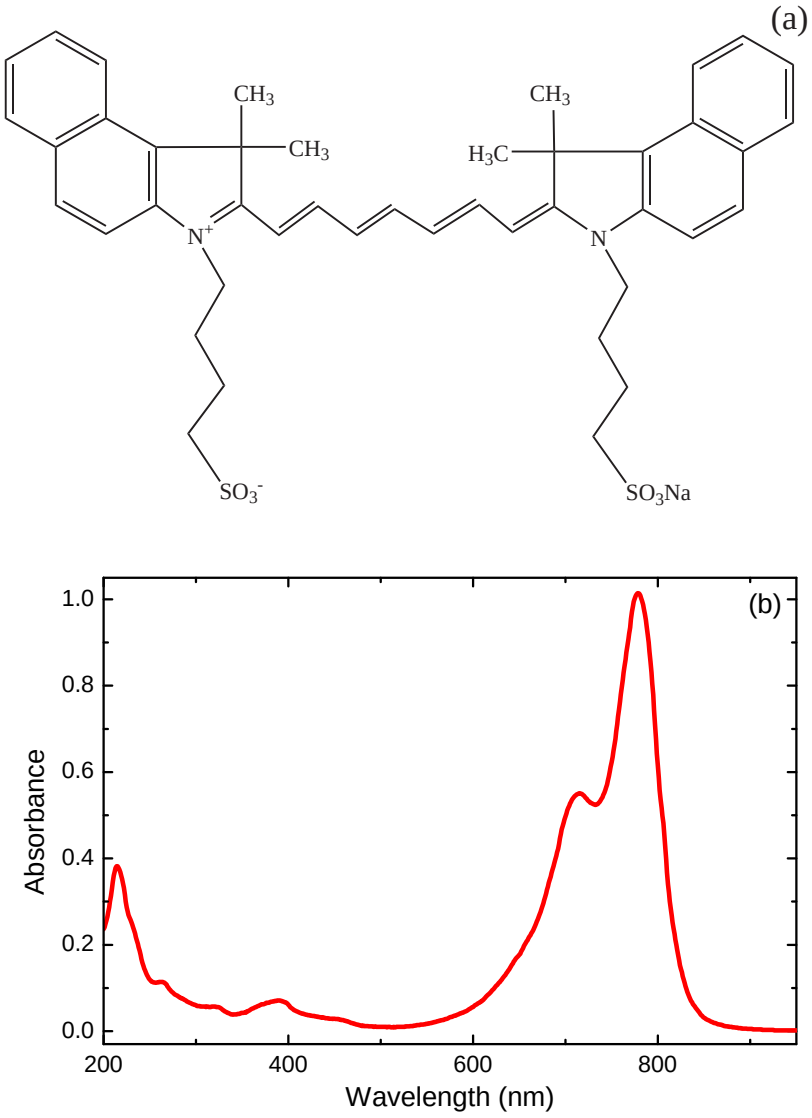

Figure 1.5: (a) Structural formula of indocyanine green. (b) Static absorption spectrum of 10 μM ICG dissolved in water. It has an absorption maximum at 778 nm.

1.3 Scope of the Thesis

The major objective of this work is to study the very initial reactions that lead to the generation of reactive oxygen species by ICG, using femtosecond time-resolved laser spectroscopy. The real-time observations of the reactions have the potential of providing new insights into the mechanism for the formation of ROS in PDT. This mechanistic understanding can improve the efficiency of currently used PDT drugs as well as develop more effective new drugs.

Following this introduction, the principle of femtosecond time-resolved laser spectroscopy is briefly described in Chapter 2.

In Chapter 3, the experimental results from the fluorescence up-conversion and pump-probe transient absorption measurements are presented and discussed. The fluorescence decay profiles of ICG was obtained from fluorescence up-conversion measurements in order to determine the lifetime of ICG excited singlet state. The transient kinetic profiles of ICG ground state recovery was measured to determine the excited triplet state quantum yield. Studies on the reaction between ICG and oxgyen was performed by using pump-probe transient absorption spectroscopy and a new reaction pathway for the generation of ROS by ICG was proposed.

Finally, the conclusions drawn from this work are summarized in Chapter 4.

Chapter 2

Experimental Technique

The major technique that has been applied in this project is the femtosecond time-resolved laser spectroscopy, which was introduced by the California Institute of Technology group of Ahmed H. Zewail into the studies of chemical reaction dynamics [69].

2.1 Pump-Probe Transient Absorption Spectroscopy

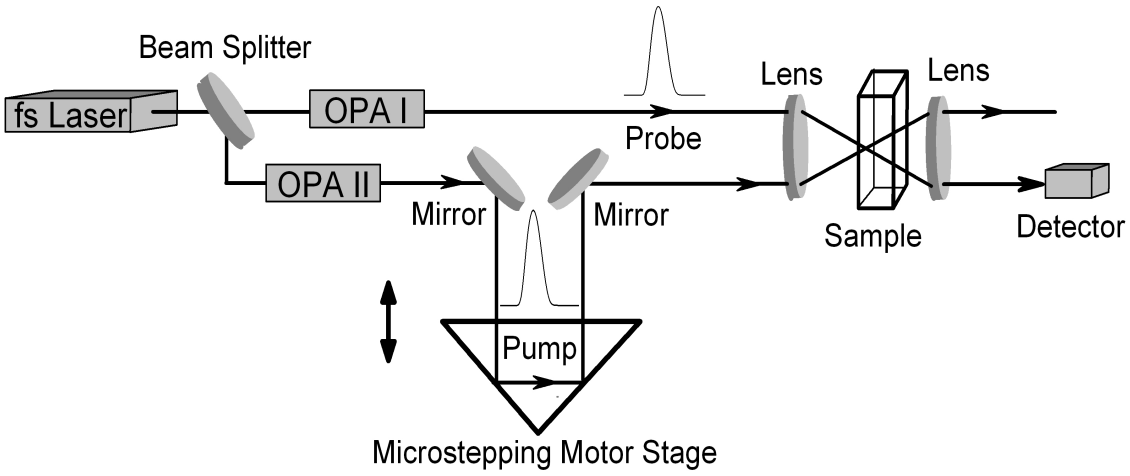

Figure 2.1: Schematic diagram of the pump-probe transient absorption spectroscopy. (OPA: optical parametric amplifier)

Figure 2.1 shows the basic setup for the pump-probe laser spectroscopy. Two laser pulses with femtosecond duration are used. The "pump" pulse is used to initiate the reaction, for example, to excite the sample molecules. The "probe" pulse at a chosen wavelength and delay time is applied to monitor the action of a specific reaction intermediate. Since each species has its own characteristic absorption peak, the behavior of different reaction intermediates can be observed by changing the probe wavelength. Different time delays between the pump pulse and the probe pulse can be achieved by varying the optical path difference (OPD) between these two pulses using a microstepping motor stage. According to the following calculation,

$$\mathrm{t} = \frac{\Delta \mathrm{s}}{\mathrm{c_{air}}} = \frac{1\ \mu\mathrm{m}}{3 \times 10^8\ \mathrm{m/s}} \approx 3.3\ \mathrm{fs},$$

an OPD of 1 μm corresponds to a time difference of about 3.3 fs. Therefore, fs time resolution can be achieved.

2.2 Fluorescence Up-Conversion Technique

Time-resolved fluorescence can be obtained by using the sum-frequency generation (SFG) technique (i.e., fluorescence up-conversion) [70]. The setup is shown schematically in Figure 2.2.

In order to achieve fs-resolution, the pump-probe technique is applied. The pump pulse is used to generate fluorescence emission. The emission from the sample is then collected by two parabolic mirrors and focused onto a BBO crystal to mix with the probe pulse which is focused at the same point on the crystal. The SFG at the crystal obeys the energy and momentum conservation laws as shown by the following equations:

$$\text{Energy conservation: } h\nu_1 + h\nu_2 = h\nu_3; \tag{2.1}$$

$$\text{Momentum conservation: } \hbar \overrightarrow{k}_1 + \hbar \overrightarrow{k}_2 = \hbar \overrightarrow{k}_3. \tag{2.2}$$

According to equation (2.1), the energy of the up-converted photon is the sum of energy of the two incident photons. Thus, the fluorescence signal if in the infrared range

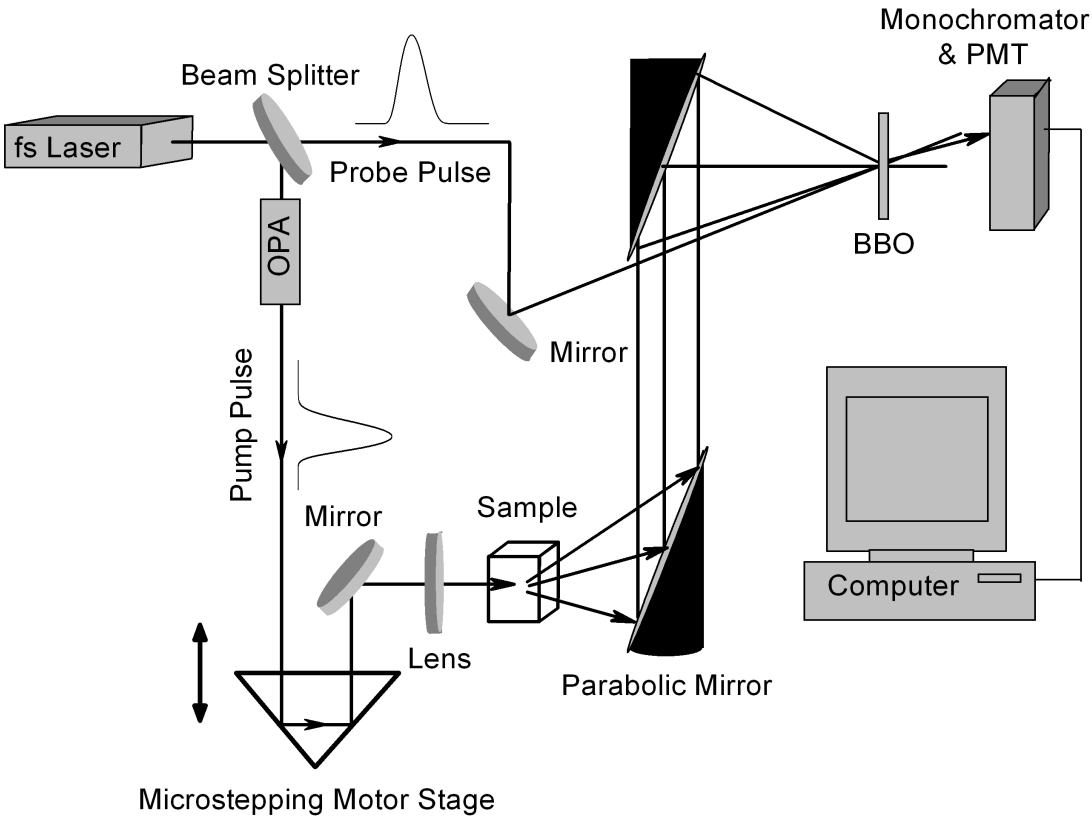

Figure 2.2: Schematic diagram of the femtosecond-resolved fluorescence up-conversion technique. (OPA: optical parametric amplifier)

can be converted to visible light and detected by photomultiplier tube (PMT) that is sensitive to visible light. Equation (2.2) is the phase matching condition which requires the BBO crystal to be set at specific orientation and angle. Therefore, the amplitude of the up-converted signal can be optimized by rotating the crystal. Finally, the up-converted signal is focused at the entrance of a monochromator and the fluorescence decay at a specific wavelength is then detected by a PMT controlled by a computer program.

2.3 Laboratory at the University of Waterloo

All the experiments of this thesis work were performed in my supervisor Dr. Qing-Bin Lu's laboratory in the Department of Physics and Astronomy, at the University of Waterloo.

In our laboratory, the standard methodology for pump-probe measurements has been applied. We used a Ti:sapphire laser system producing 100-120 fs, 1 mJ laser pulses centered at 800 nm with a repetition rate of 1 kHz. Two optical parametric amplifiers (OPA) capable of generating pulses with wavelengths from ultra violet (UV, $\lambda \geq 266$ nm) to near infrared (NIR, several micrometers) were used to produce the pump and probe pulse respectively. The polarization of the pump and probe pulses was set at the magic angle 54.7° in order to avoid contribution from polarization anisotropy due to rotational diffusion of the molecules [71]. Pump energies ≤ 200 nJ were used. The pump and probe wavelengths of specific measurements are given together with the results. The electronic devices detecting the signals and the motion controller are integrated into Labview programs that can directly give the time-resolved absorption or fluorescence kinetic traces.

All decay kinetic traces were fitted to a number of exponential functions by using a least-squares fitting program. These exponential terms were convoluted with the instrument-response function represented by a Gaussian function.

All transient absorption and fluorescence measurements were performed at room temperature in a 5 mm quartz cell with a magnetic stirring bar. All samples were stirred during measurements to avoid product accumulation.

Ultrapure water with a resistivity of >18 MΩ/cm obtained directly from a Barnstead Nanopure water system was used.

All static absorption spectra were measured with a UV/Visible/NIR spectrophotometer (Beckman, life sciences).

Chapter 3

Molecular Reaction Pathway for the Generation of ROS in PDT with Indocyanine Green

3.1 Introduction

Photodynamic therapy (PDT) is a potential clinical approach for the treatment of numerous cancers such as the cancers of the bladder [31], prostate [32], and lung [4], as well as some other nonmalignant conditions such as psoriasis [72] and age-related macular degeneration (ARMD) [73, 74]. The requirement of the coexistence of both the photosensitizer and light to cause tissue damage enables precise control of PDT treatment [75]. The therapeutic effect of PDT is believed to be mainly from the reactive oxygen species (ROS) generated by the reaction of the excited photosensitizing drug molecule with oxygen [11]. Although a few PDT sensitizers have been approved for clinical uses, the molecular mechanisms for drug action, especially the generation of ROS, are poorly understood. Moreover, currently used photosensitizers are activated within the wavelength range of 630 to 690 nm. In this wavelength range, the PDT efficiency of these drugs is limited by the tissue penetration depth of light [11]. One of the approaches to improve the therapeutic effectiveness of PDT is to develop new drugs that are sensitive to near infrared (NIR) light.

Indocyanine green (ICG), which has a strong absorption band between 700 nm and 800 nm coincident with the human tissue optical window [12], is a potential NIR PDT sensitizer. Indocyanine green-induced photo-oxidative killing of human cancer cells has been reported [63–65]. The conventional mechanism of PDT gives that the ROS are generated from the excited triplet state of the photosensitizer through photodynamic reaction of either type I or type II [11], as described in Chapter 1. According to this mechanism, the photosensitizing drug should have a high quantum yield and long lifetime of the triplet state in order to induce significant cancer cell damages. Thus, for PDT studies, there is a strong need for knowing the triplet state yield of ICG. However, not much information can be found in the literature, perhaps because of the well known property of cyanine dyes to have low singlet-triplet intersystem crossing yields [76]. For example, the maximum Φ_T in methanol for carbocyanines was found to be about 3% [77]. In 1997, Reindl *et al.* determined the triplet state yield of ICG-NaI in various media including DMSO (0.17), methanol (0.16), water (0.14) and aqueous albumin solution (0.11) using a picosecond laser double-pulse fluorescence excitation technique [78]. Later in 1999, the same group obtained a yield of $\Phi_T = 1.7 \times 10^{-6}$ in nitrogen-bubbled water by theoretical fitting to the experimental transmission of the sample [67]. They also came to the conclusion that indocyanine green solutions were inefficient for triplet-state induced cell damage in PDT applications. However, the approaches they have applied in these two studies for the determination of excited triplet-state yield relies on several assumptions and, therefore, are indirect. No direct determination of Φ_T of ICG was reported until 2007; the quantum yield of the excited triplet state of ICG in methanol was found to be extremely low by Sudeep *et al.*, in their study of the photo-induced electron ejection from the excited state of ICG into TiO_2 and $Ag@TiO_2$ core shell nanoparticles [68].

Although Sudeep *et al.* have obtained direct evidence for the absence of long-lived species, their measurements were performed in methanol instead of in aqueous solution which is closer to a biological environment. More importantly, they did not discuss the generation of ROS by ICG. Therefore, we feel it is still of great importance to study the behaviors of ICG in water solutions. Moreover, with our femtosecond time-resolved laser spectroscopy, we are capable of studying the very initial reactions that may lead to the generation of ROS in PDT, since ICG was found to have a fluorescence lifetime shorter than 160 ps in water [79]. In this work, we performed a series of experiments on ICG in aqueous solutions, including fluorescence up-conversion measurements and studies of

the ground state bleaching, the reaction with oxygen, as well as the concentration effects. This study should be able to improve our understanding of the molecular mechanism of PDT.

3.2 Determination of Molar Extinction Coefficient of ICG

The dye indocyanine green (ICG) is a water-soluble tricarbocyanine dye developed in the Kodak Research Laboratories in 1955. Since its approval by the United States Food and Drug Administration (FDA) in 1956, ICG has been widely used in medical diagnosis [55–60, 80, 81]. Despite it's popularity, the application of ICG is limited due to the tendency to aggregate, which is the most notable property of the cyanine dyes. Stability of ICG in aqueous solution has been studied a lot [61, 82–87]. The concentrated solutions were found to be stable for only 2 days after preparation. A new absorption maximum at 900 nm, which is caused by the formation of J-aggregation, can be formed in about 7 days after sample preparation [61]. Thus, it is necessary to prepare fresh ICG samples daily in order to avoid any possible contribution from the aggregation state in the samples.

The Beer-Lambert's law states that the absorption of light at a certain wavelength (λ) is directly proportional to the solute concentration (c in M) and the length of the light path (b in cm), i.e.

$$A = \varepsilon \times b \times c, \tag{3.1}$$

where ε in $\mathrm{cm}^{-1}\mathrm{M}^{-1}$ is the molar extinction coefficient. According to equation (3.1), the absorbance of a solute at a fixed wavelength is proportional to its concentration. In other words, the absorbance and the concentration have a linear relation. Therefore the concentration of a solution with known ε values can be determined by measuring it's absorbance using a spectrophotometer.

It will be more precise to determine the concentration of the stock solution by using the molar extinction coefficient than from the weight of the solute since only a small amount of sample (less than 1 mg) is needed for one day's use. Thus for the purpose of sample concentration control, we determined the molar extinction coefficient of ICG in water.

3.2.1 Experimental details

ICG (molecular weight 774.98) was purchased from Sigma-Aldrich and used as supplied. A stock solution of 1 mM was prepared by dissolving 1.1 mg ICG powder in 1.419 ml ultrapure water. Static absorption spectra of diluted samples with concentrations of 1, 2, 3, 4, 5, 10, and 20 μM, respectively, were then measured by using a UV/Visible/NIR spectrophotometer (Beckman, life sciences).

3.2.2 Results and discussion

The Beer-Lambert's law is obeyed in a certain range of concentration. In the case of ICG, the departure from the Beer-Lambert's law becomes significant when the sample concentration is higher than 10 μM (in water) due to the formation of H-aggregation [83, 88]. Therefore, only the results of samples with concentrations of 1, 2, 3, 4, and 5 μM were used to determine the ε value.

Figure 3.1(a) shows the static absorption spectra of these ICG samples. Figure 3.1(b) is the plot of the absorbance value at 778 nm against the sample concentration. According to equation (3.1), a linear relation between the absorbance value and the sample concentration should be obtained. A linear fit to the experimental data gave a slope of $k = 0.224$ with an R^2 of 0.9997. So the molar extinction coefficient of ICG dissolved in water can be calculated using the following equation:

$$\varepsilon_{778\text{ nm}} = \frac{k}{b} = \frac{0.224\ \mu\text{M}^{-1}}{1\text{ cm}} = \frac{0.224 \times 10^6\ \text{M}^{-1}}{1\text{ cm}} = 2.24 \times 10^5\ \text{cm}^{-1}\text{M}^{-1}.$$

This value agrees well with the reported value of $\varepsilon = 2.05 \times$ $\text{cm}^{-1}\text{M}^{-1}$ in water [89] and, therefore, was used to control the concentration of the samples in later experiments.

3.3 Fluorescence Up-Conversion Measurements

Fluorescence measurements are the most direct way for the determination of the S_1 state lifetime, without contribution from vibrational relaxation and solvation effects. With

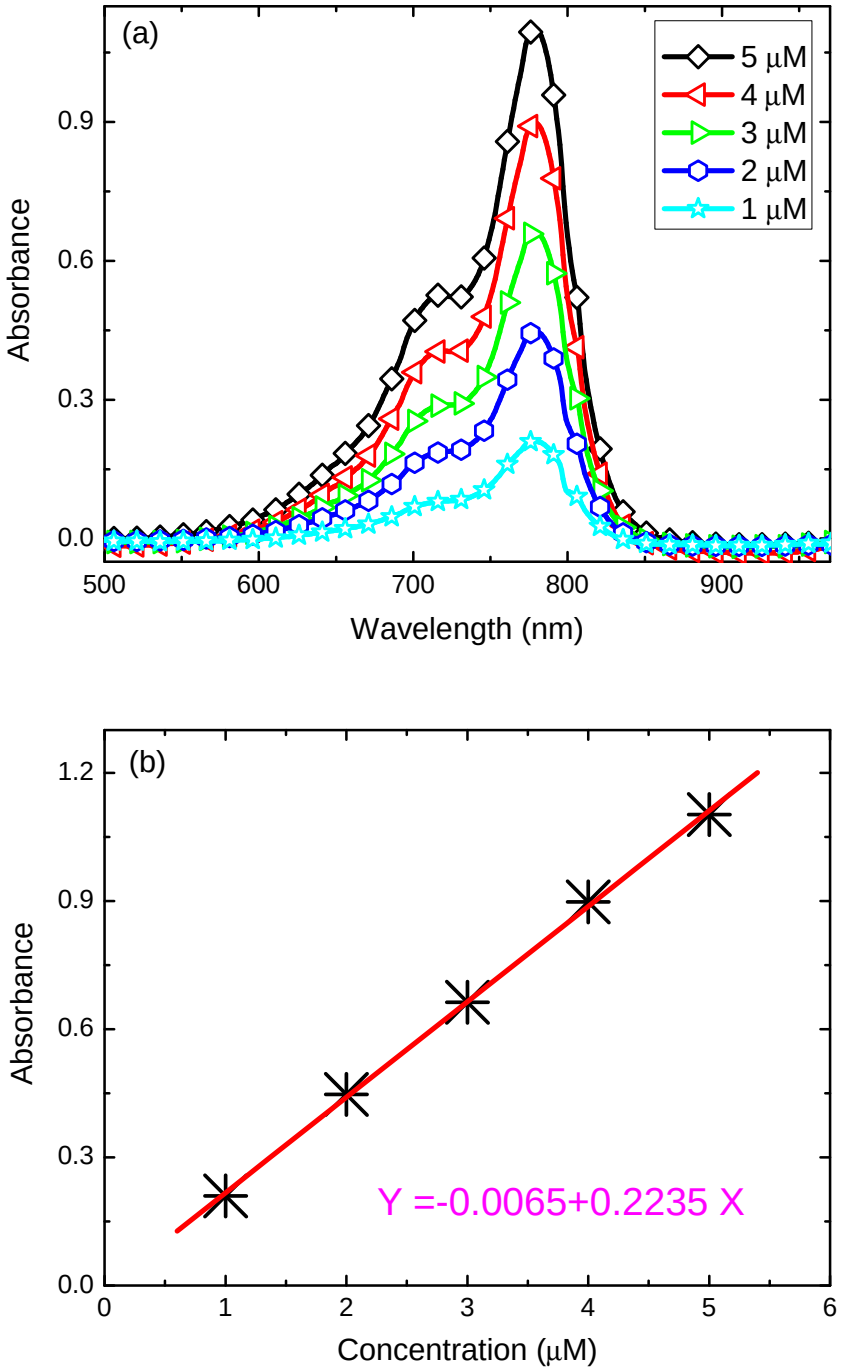

Figure 3.1: (a) Static absorption spectra of various concentrations of ICG (1, 2, 3, 4, and 5 μM) in water measured in 1 cm polystyrene cuvettes. (b) Plotting of the absorbance value at 778 nm as a function of the sample concentration. A linear fitting to the experimental data gives a slope of 0.224 with an R^2 of 0.9997.

our fs laser spectroscopy, we have performed femtosecond time-resolved fluorescence studies on ICG using fluorescence up-conversion technique which is extremely attractive for time-resolved fluorescence studies due to the availability of excellent photomultiplier tubes (PMTs) in the UV and blue regions.

3.3.1 Experimental details

ICG samples with a concentration of 25 μM were diluted from a stock solution of 1.13 mM. The excitation wavelength was set at 800 nm and the pump pulse energy was 200 nJ. The collected fluorescence emission was mixed with the probe pulse set at 800 nm to generate the up-converted signal. A blue bandpass filter (BG40, Newport Corporation) was place in front of the monochromator to allow the up-converted light to pass through and block the fluorescence light as well as the 800 nm light. The fluorescence decay kinetics at three different wavelengths, i.e. 870 nm, 900 nm, and 930 nm were recorded by setting the monochromator at 417 nm, 424 nm, and 430 nm respectively. Fluorescence of shorter wavelengths were not measured since there was more contribution from the 400 nm light generated by the crystal from the probe pulse than that from the up-converted fluorescence signal at these wavelengths. For wavelengths longer than 930 nm, fluorescence profiles were not measured since the signal became too weak to get a high signal-to-noise ratio.

3.3.2 Results and discussion

Fluorescence decay kinetic traces of ICG at three different wavelengths are presented in Figure 3.2. All decays were adequately fitted by a single-exponential function and the decay lifetime was determined to be 155 ps, 147 ps, and 145 ps, respectively. Attempts to fit the data to a double-exponential function did not give better results. This lifetime of around 150 ps was attributed to be the lifetime of the excited singlet state of ICG. No long-lived species were observed in this experiment.

Studies on the fluorescence properties of ICG in various media can be found in the literature [79, 88]. Soper *et al.* determined the fluorescence lifetime of ICG in methanol,

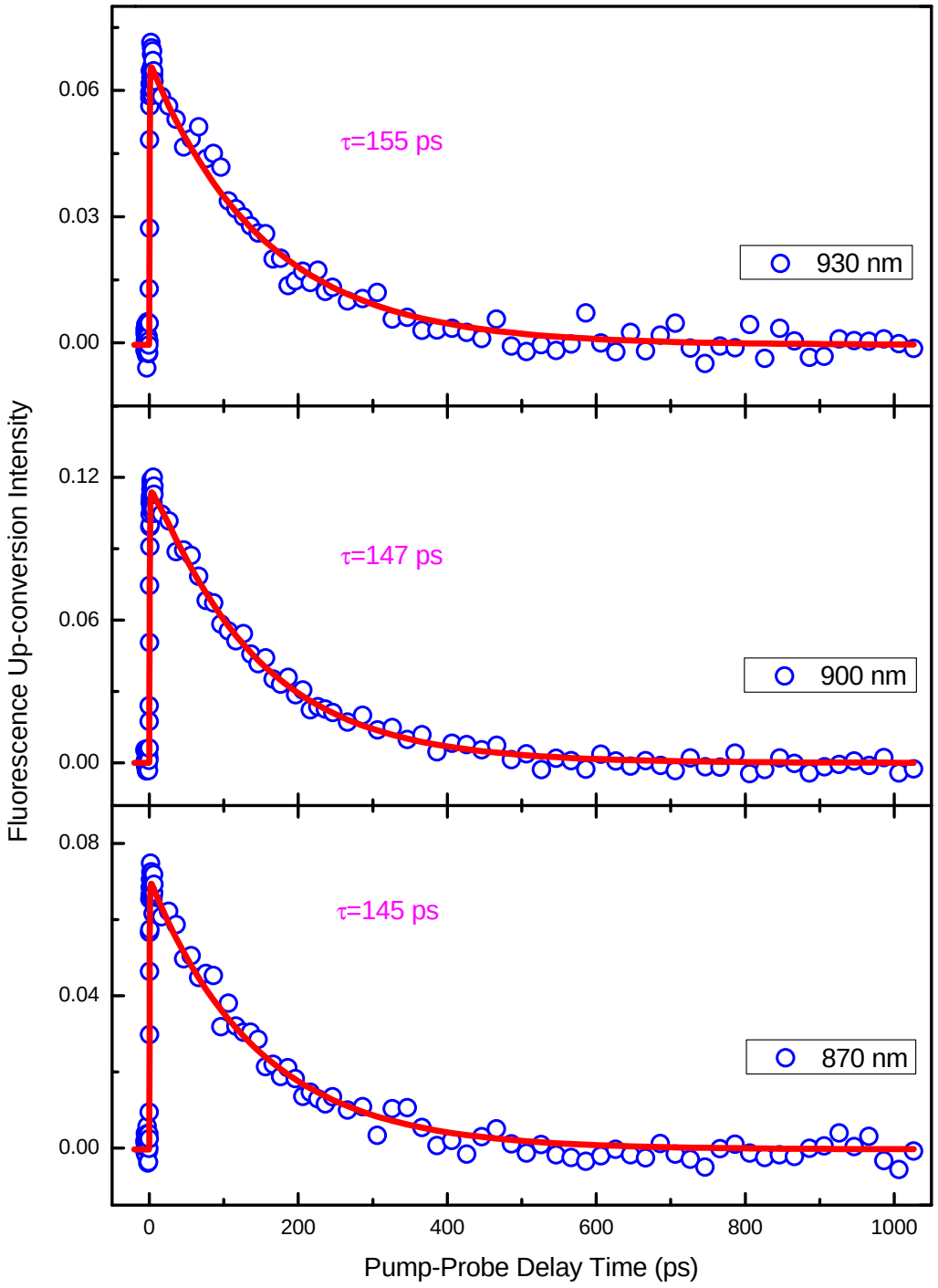

Figure 3.2: Femtosecond time-resolved fluorescence decay kinetic traces of 25 μM ICG in water at three different wavelength. The excitation wavelength was 800 nm with an energy of 200 nJ. The solid lines are the best fits to the experimental data.

water, methanol/water binary mixture, D_2O, SDS and Triton X-100 directly from the fluorescence decay profiles [79]. They reported a τ_F value of 470 ps in 100% of methanol and $\tau_F = 160$ ps in a binary mixture consisting of 75% of H_2O and 25% of methanol. Unfortunately, the lifetime of ICG in 100% water could not be determined with the resolution of their NIR time-correlated single photon counting (TCSPC) device. In 1996, Philip *et al.* calculated a fluorescence lifetime of 20 ps in water [88]. However, in this report, the τ_F value in methanol was determined to be 190 ps which was much shorter than 470 ps reported in Ref .[79]. Moreover, Sudeep *et al.* have obtained a $\tau_F = 410 \pm 10$ ps (in methanol) [68] consistent with the value of 470 ps in Ref .[79] rather than 190 ps in Ref .[88]. This difference is probably due to the different approaches used. Philip *et al.* obtained their values through complicated calculations using their fluorescence quantum distributions data while Soper *et al.* and Sudeep *et al.* determined the lifetime directly from the decay profiles.

We are the first to obtain fluorescence decay profiles of ICG in water by using our femtosecond time-resolved fluorescence up-conversion spectroscopy. The lifetime of $^1ICG^*$ have been determined to be around 150 ps.

3.4 Ground State Recovery of ICG

The determination of the excited triplet state quantum yield of the photosensitizer is especially important for PDT applications. Numerous procedures have been developed including fluorescence quenching [90], triplet-sensitized isomerization [91], delayed fluorescence measurements [92], electron spin resonance [93], laser flash absorption and relative actinometry [94], and time-resolved photothermal techniques [95]. However, these methods have their disadvantages since they often rely on very careful calibration, an external standard, or measurements performed in ratio mode such as comparison of fluorescence intensities. Lament *et al.* have developed a simple procedure for the determination of Φ_T which uses transient kinetic profiles of ground state recovery of the compound under investigation and thus avoids the need for a relative measurement [96].

Figure 3.3 shows the principle of ground state bleaching measurements. Without excitation, all molecules are in the ground state (as shown in Figure 3.3(a)). When the

pump pulse comes, some of the molecules get excited and go to the excited singlet state resulting in a decrease of the number of molecules in the ground state (Figure 3.3(b)).

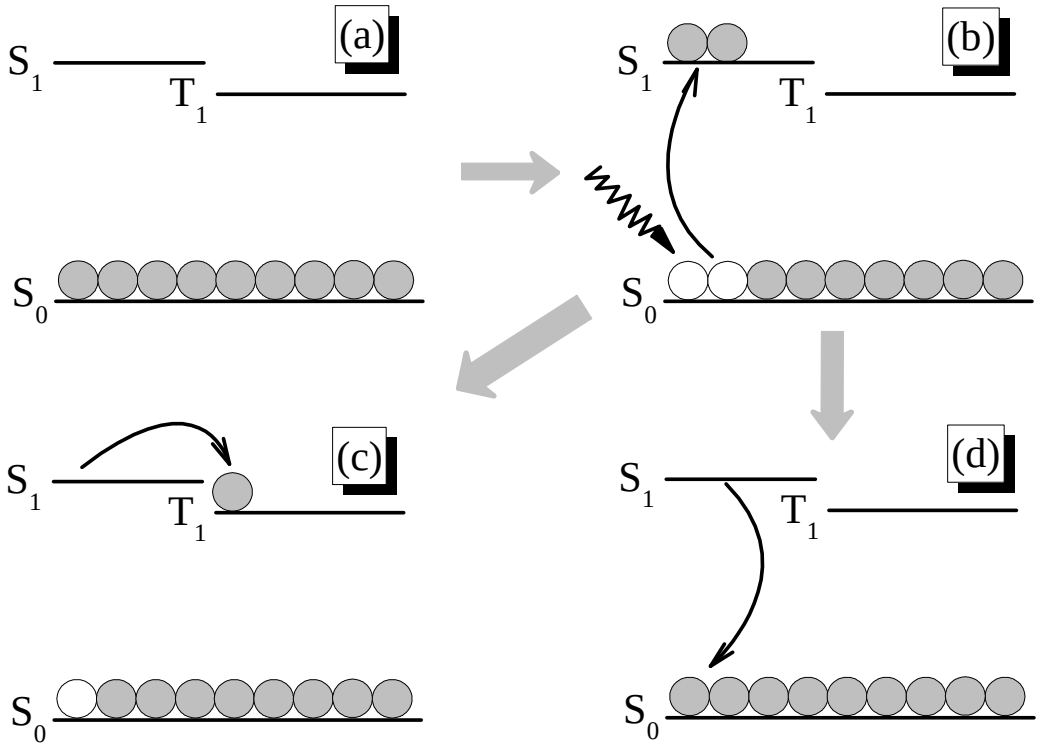

Figure 3.3: Schematic diagram showing the principle of ground-state bleaching measurements.

This will give rise to a decrease in the absorbance at specific wavelengths where the molar extinction coefficient of the ground state is much higher than that of the excited state. Thus a negative signal is generated. The recovery of this negative signal corresponds to the relaxation of the excited molecules back to the ground state (Figure 3.3(d)). A 100% recovery will be observed if all the molecules go back to S_0 within the time of the measurement. However, a 100% recovery can not always be achieved if a large number of molecules go to the long-lived T_1 state through a process called inter-system crossing (ISC) (Figure 3.3(c)).

3.4.1 Experimental details

ICG sample with a concentration of 10 μM was diluted from a stock solution of 256 μM. In this experiment, the probe wavelength was set at 800 nm, where the absorption of the ground state of ICG is dominating, and the pump wavelength was 400 nm, with an energy of 40 nJ.

3.4.2 Results and discussion

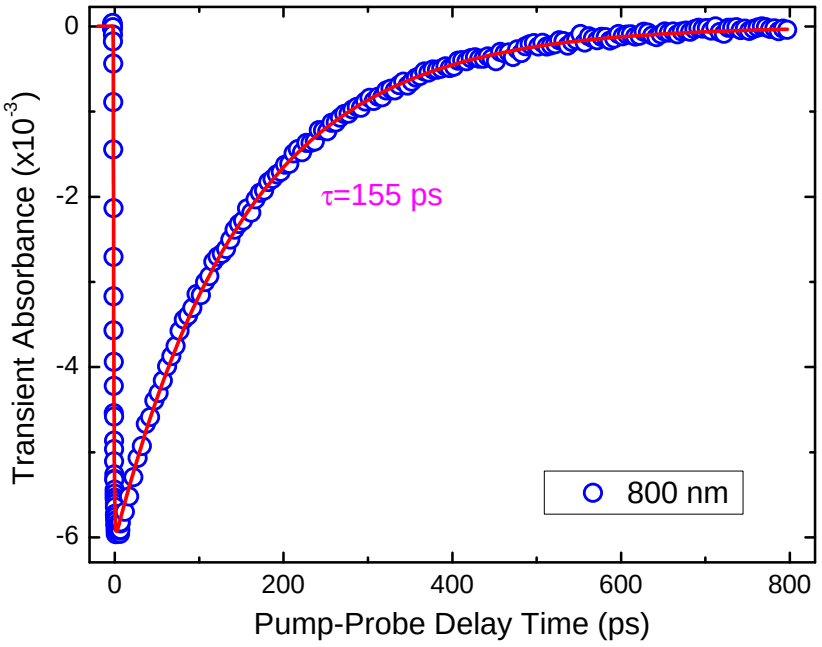

Figure 3.4: The ground-state bleaching recovery trace of 10 μM ICG in water. The pump wavelength was 400 nm with an energy of 40 nJ and the probe wavelength was 800 nm. The solid line is the best fit to the experimental data, giving a decay time of τ=155 ps. The recovery of ICG ground-state at the time delay of 800 ps was calculated to be 99.4%.

The result is shown in Figure 3.4. The best fit to the experimental data gives a single recovery lifetime of 155 ps, which is consistent with the lifetime of ICG excited singlet state obtained from fluorescence measurement. In addition, a recovery of about 99.4% was achieved at the time delay of 800 ps. These results indicate that ICG has an extremely low quantum yield of excited triplet state ($\Phi_{^3ICG^*} < 0.6\%$) in water.

The result of this experiment confirms that the lifetime of ^{1}ICG* in water is about 150 ps rather than the reported value of 20 ps [88].

A low quantum yield of the excited triplet state of ICG is expected [67, 76]. Values of Φ_T have been reported previously [67, 68, 78]. By using a picosecond laser double-pulse fluorescence excitation technique [97], Reindl *et al.* were the first to measure the quantum yields of ICG in various media including DMSO, methanol, water, and aqueous albumin solution. The reported Φ_T values of ICG in water and methanol were 0.14 and 0.16 respectively [78]. However, later in 1999, the same group reported different values of $\Phi_T = 1.7 \times 10^{-6}$ (in water) and $\Phi_T = 2.3 \times 10^{-5}$ (in methanol), and concluded that ICG was inefficient for PDT applications [67]. No explanation was given about the inconsistence of the values. More recently, Sudeep *et al.* obtained the bleaching trace of ICG in methanol at 750 nm which suggested the absence of long-lived species [68]. Our studies on the ground-state recovery of ICG shows that Φ_T in water is also extremely low.

Considering it's low yield of excited triplet state, we can rule out the following two possible reaction pathways that may contribute to the generation of ROS by ICG.

$$^3\text{ICG}^* + ^3\text{O}_2 \rightarrow \text{ICG} + ^1\text{O}_2; \tag{3.2}$$

$$^1\text{ICG}^* + ^3\text{O}_2 \rightarrow ^3\text{ICG}^* + ^1\text{O}_2. \tag{3.3}$$

Both reactions involve the ^{3}ICG*. Reaction (3.2) involves energy transfer from ^{3}ICG* to ground state oxygen to produce ^{1}O$_2$. Since the quantum yield of ^{3}ICG* has been found to be extremely low, it is unlikely that large amount of ^{1}O$_2$ could be generated through this pathway. Reaction (3.3) is the generation of ^{1}O$_2$ from ^{1}ICG*. If this reaction did take place, large amount of ^{3}ICG* should have been produced too, which was not observed. So this reaction can also be ruled out. Then for photosensitizers with low triplet state quantum yields such as ICG, there might exist a new reaction pathway for the generation of ROS which does not involve the long-lived excited triplet state of those compounds.

3.5 Reaction Between ICG and Oxygen in Water

Femtosecond time-resolved transient absorption laser spectroscopy is one of the most powerful technique for direct examination of the reaction dynamics [69]. In order to reveal the molecular mechanism for the generation of the ROS in ICG-mediated PDT, we performed real-time studies on the reaction between ICG and O_2 in water.

3.5.1 Experimental details

In this experiment, two 10 μM ICG samples were diluted from a stock solution of 884 μM and bubbled with O_2 and N_2, respectively. Transient absorption decay kinetic traces were measured for both samples immediately after bubbling. Static absorption spectra of both samples were recorded too. In the following day, both transient absorption decay kinetic traces and static absorption spectra of these two samples were recorded again after being kept in dark at 4 °C for 17 hours. In the transient absorption measurements, the pump was set at 800 nm with an energy of 48 nJ and the probe wavelength was 615 nm.

3.5.2 Results and discussion

Figure 3.5(a) shows the original data of femtosecond time-resolved transient absorption decay kinetic traces of all the samples. We noted that the intensity of the initial peaks of both samples decreased by $\sim 40\%$ after being kept in dark for 17 hours. This was due to a decrease in the sample concentration [61, 82]. To eliminate this concentration effect, all curves were normalized to their initial peaks. The normalized traces (Figure 3.5(b)) showed no difference between the O_2-bubbled sample and the N_2-bubbled one immediately after the bubbling. However, a dramatic change in the sample with O_2 could be seen after being kept in dark for 17 hours, while there was no significant change in the sample with N_2.

The normalized static absorption spectra of all these samples are shown in Figure 3.6. A broadening of the absorption band and an enhancement of the absorption at $\sim$710

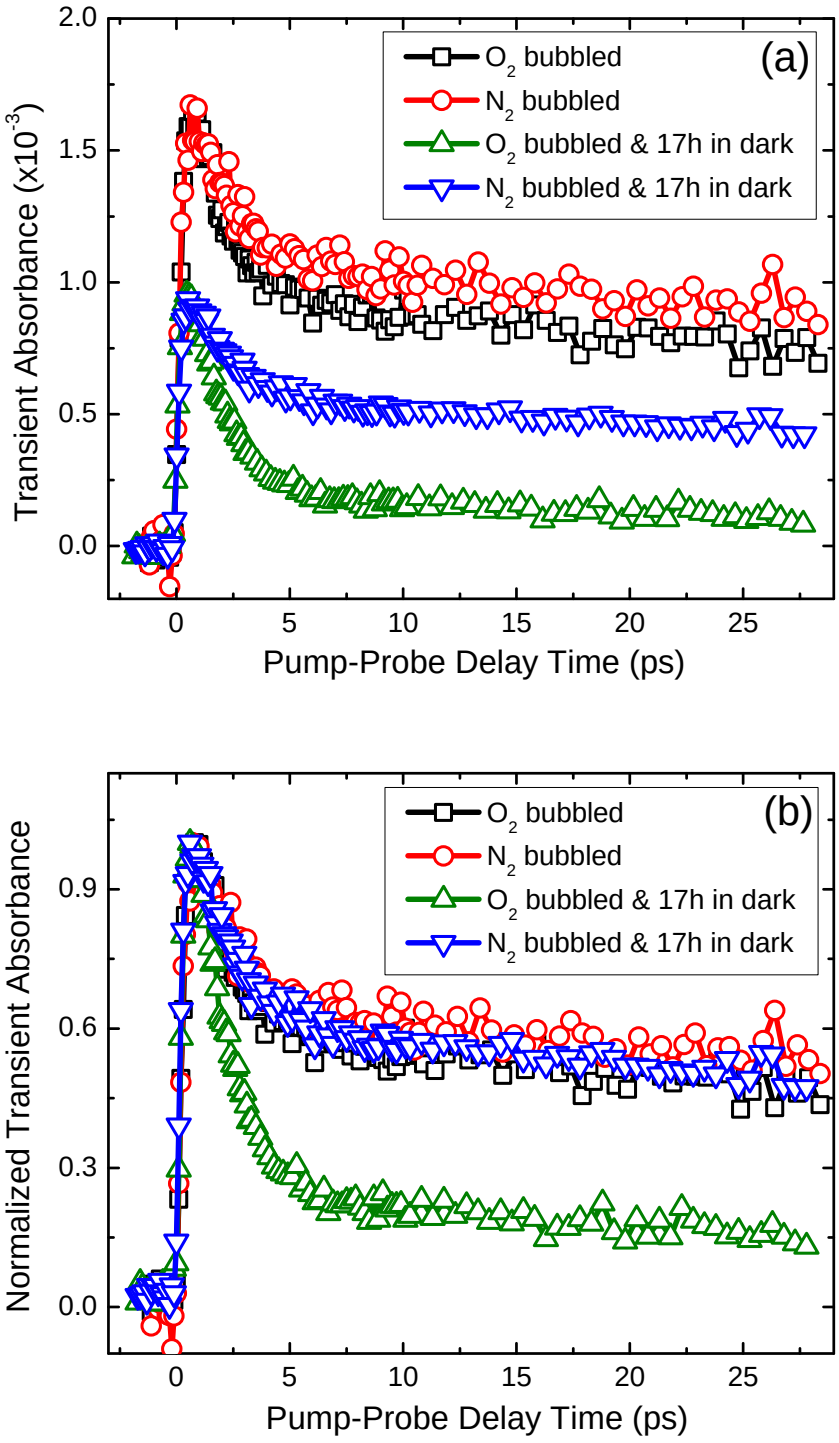

Figure 3.5: (a) is the original data of the femtosecond time-resolved transient absorption decay kinetic traces of 10 μM ICG in water. (b) is the transient absorption decay kinetic traces normalized at the initial peaks. The pump wavelength was 800 nm with an energy of 48 nJ and the probe wavelength was 615 nm.

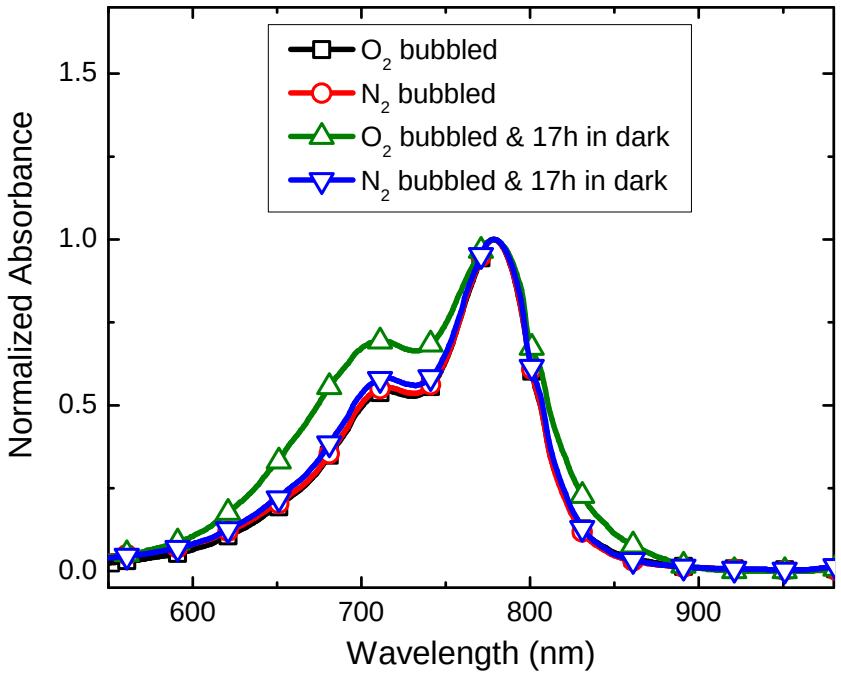

Figure 3.6: The normalized static absorption spectra of all the samples.

nm were clear for the O_2-bubbled sample after being kept in dark for 17 hours. These results indicated the existence of interactions between ICG and O_2 in the ground state. However, we noted that the enhanced absorption at $\sim$710 nm was similar to the behavior of ICG H-aggregation, which was characterized by a blue shift in the main absorption peak [98]. Thus further studies were required in order to determine whether the change of ICG sample in the presence of O_2 was due to the formation of the H-aggregation.

3.6 Concentration Effect of ICG in Water

Indocyanine green easily aggregates in aqueous solutions; the H-aggregate states can be obtained simply by increasing its concentration [61, 88]. Therefore, we studied the concentration effect of ICG in water in order to determine whether the change in the transient absorption signals is related to the formation of H-aggregation.

3.6.1 Experimental details

In this experiment, three ICG samples with concentrations of 3, 5, and 10 μM were diluted from a stock solution of 244 μM. Both the transient absorption decay kinetic traces and the static absorption spectra of all three samples were recorded. In the transient absorption measurements, the pump pulse was set at 800 nm with an energy of 48 nJ and the probe wavelength was 615 nm.

3.6.2 Results and discussion

Both the transient and static absorption curves of all three samples (3, 5, and 10 μM) have been obtained. The normalized static absorption spectrum of the 10 μM sample showed an enhanced absorption at $\sim$710 nm (Figure 3.8(b)) indicating the existence of ICG H-aggregation in this sample. However, no difference among these samples was observed in the normalized transient absorption signals (Figure 3.7(b)). This result suggested that the H-aggregate states of ICG had no contribution to the transient absorption measurements performed earlier. Thus the change in the transient kinetic trace observed in the sample with O_2 did not involve the formation of the H-aggregate states; it implied the interaction between ICG and O_2. This interaction was assigned to be the formation of ICG and O_2 complexes in their ground states ($[ICG]_m$:$[O_2]_n$) based on the fact that the change was significant only when the sample had been kept for a long time in the presence of O_2. The formation of the $[ICG]_m$:$[O_2]_n$ might be able to induce a broadening of the static absorption band as well.

3.7 Transient Absorption Spectra of ICG

The ICG and oxygen complexes, if formed, should exhibit distinct absorption characteristics. All the transient absorption kinetic profiles obtained (Figure 3.5 and Figure 3.7) showed two distinct decay components indicating the existence of two transient species. Therefore, we also performed transient absorption spectra measurements to obtain the transient absorption kinetics of ICG at different probe wavelengths.

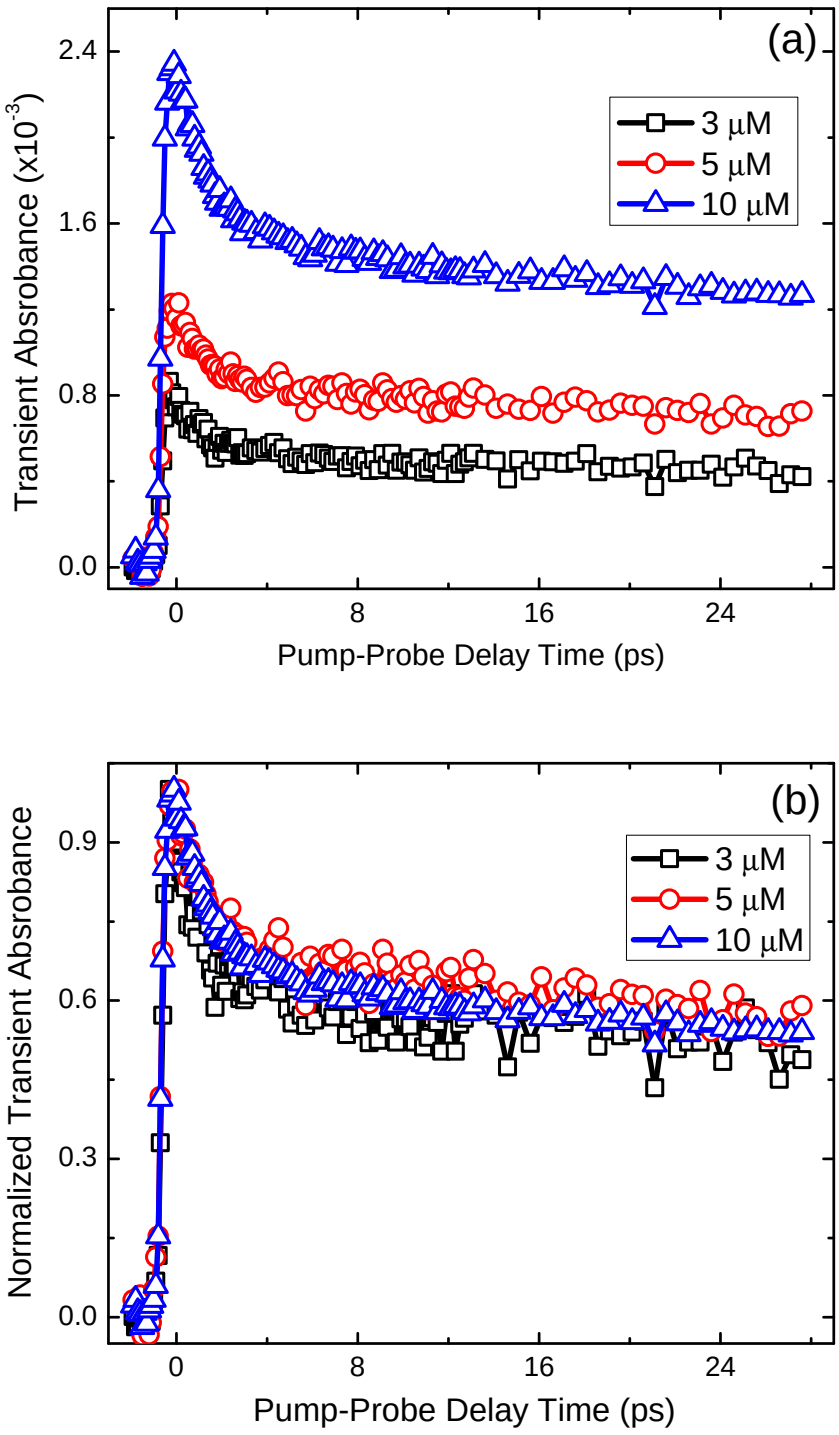

Figure 3.7: Femtosecond time-resolved transient absorption decay kinetic traces of three different concentrations of ICG (3, 5, and 10 μM) in water: (a) shows the original data; (b) shows the normalized traces. The pump wavelength was 800 nm with an energy of 48 nJ and the probe wavelength was 615 nm.

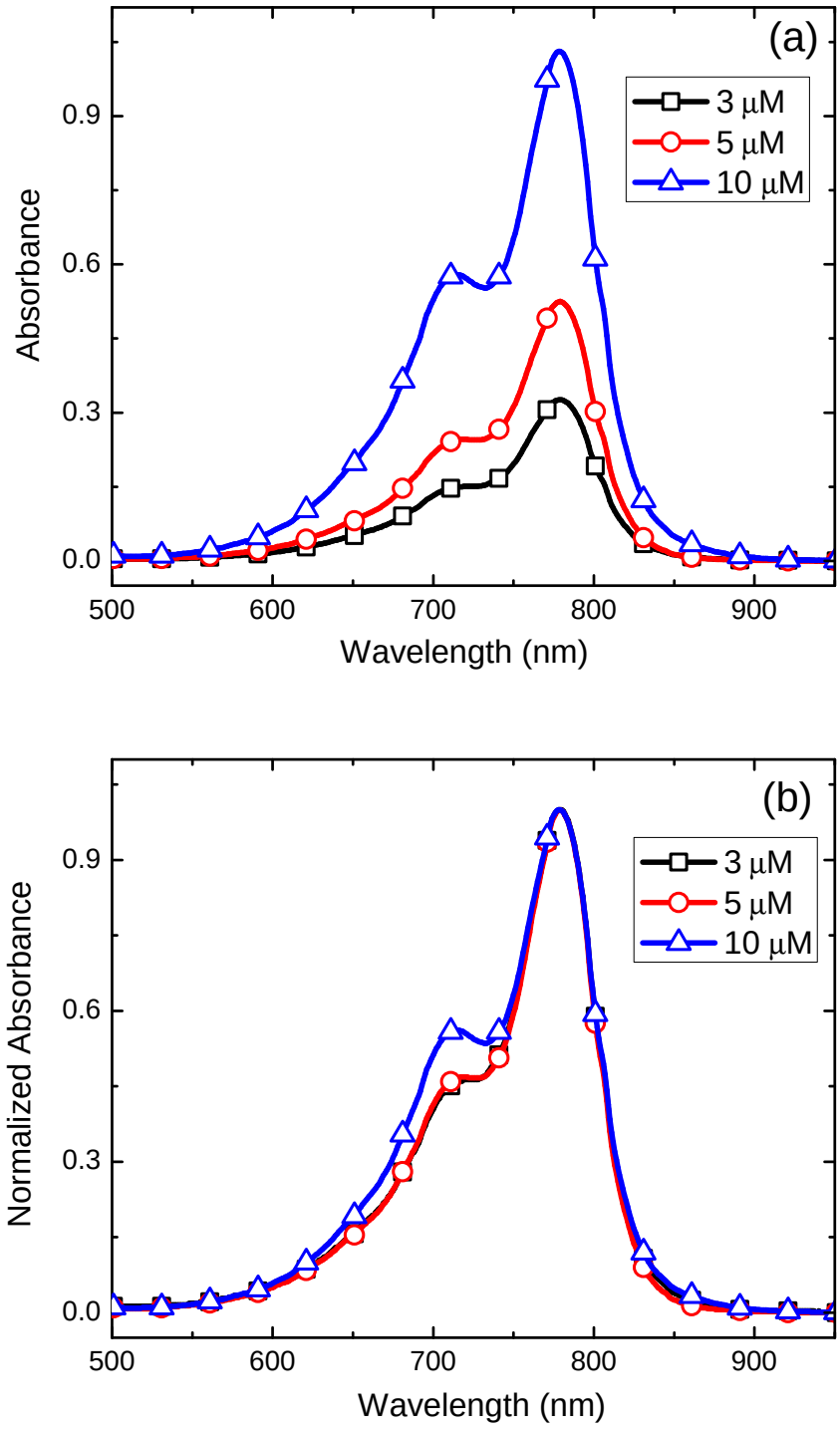

Figure 3.8: Static absorption spectra of three different concentrations of ICG (3, 5, and 10 μM) in water: (a) shows the original data; (b) shows the normalized spectra.

3.7.1 Experimental details

The setup in this experiment was similar to that of the pump-probe absorption spectroscopy described earlier in Chapter 2 with the following modifications:

1. A white light continuum (WLC) probe was used instead of the single color pulse.
2. A monochromator was used to select the wavelength.
3. The photodiode detector was replaced by a photomultiplier tube.

In order to obtain the transient absorption spectra at a specific time delay, we moved the microstepping motor stage to a certain position and then made the monochromator to do wavelength scanning. When measuring the transient absorption decay traces, we set the monochromator to a specific wavelength and moved the microstepping motor stage to get the time-resolved results.

ICG samples with a concentration of 30 μM were diluted from a stock solution of 1 mM which had been kept in dark for 2 days. The pump wavelength was 800 nm with an energy of 200 nJ. The step of the monochromator was 3 nm for the transient absorption spectra measurements.

3.7.2 Results and discussion

Femtosecond time-resolved transient absorption spectra of 30 μM ICG in water at different five pump-probe time delays following the laser pulse excitation are shown in Figure 3.9. The absorption spectra covers the whole visible range with an absorption maximum at about 560 nm. The negative absorption starting from $\sim$620 nm comes from the strong absorption of the dye molecules in the ground state. The normalized spectra (Figure 3.9 (b)) shows that the absorption intensity does not decrease monotonically at all probe wavelengths, suggesting the existence of two distinct species in this sample.

In order to determine the lifetimes of this two species, we also measured the femtosecond time-resolved transient absorption decay kinetic traces of ICG samples at four different wavelengths (i.e. 500 nm, 520 nm, 560 nm, and 600 nm) (Figure 3.10).

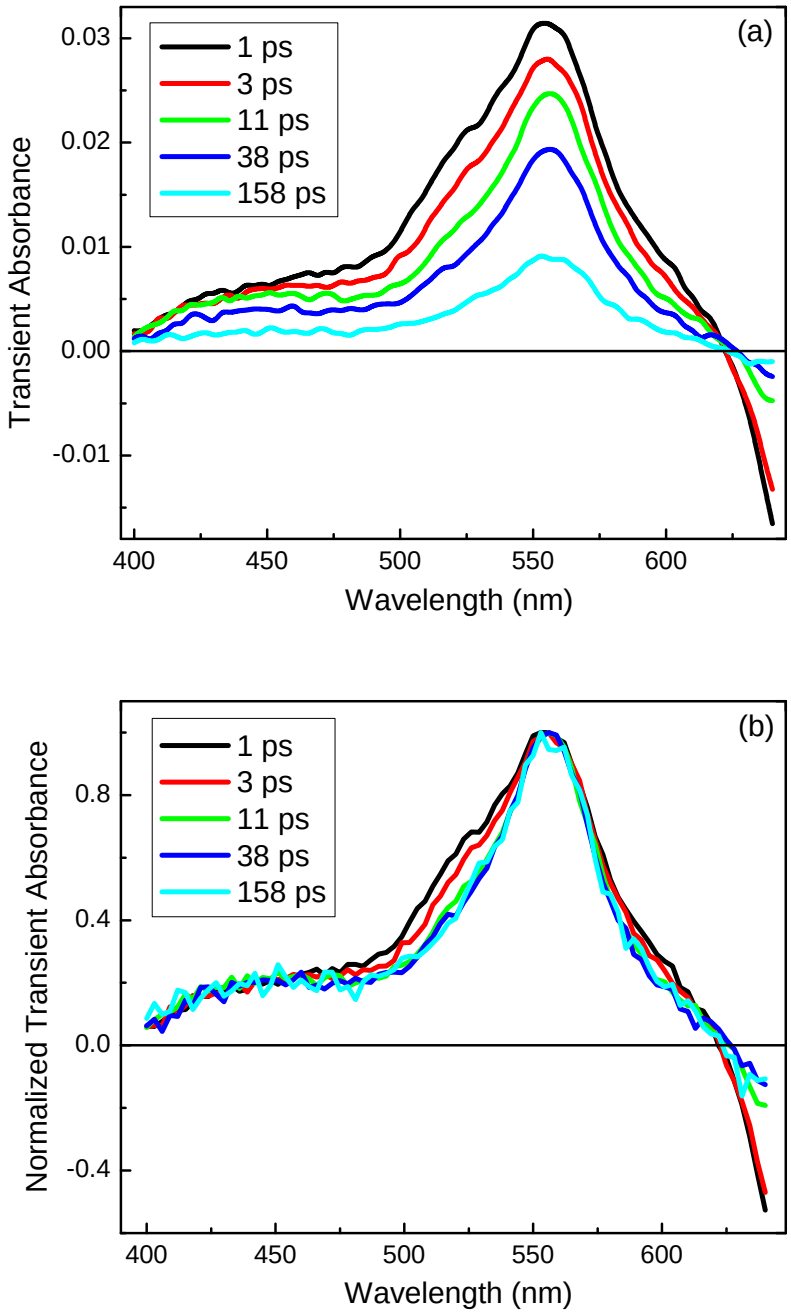

Figure 3.9: Femtosecond time-resolved transient absorption spectra of 30 μM ICG in water recorded at the visible region. The pump wavelength was 800 nm with an energy of 200 nJ and the probe pulse was white light continuum. The spectra were measured at five different pump-probe time delays following excitation. (a) are the original data showing that the excited singlet state of ICG has a broad absorption band in the visible range, with a absorption peak at 560 nm. (b) are the normalized spectra.

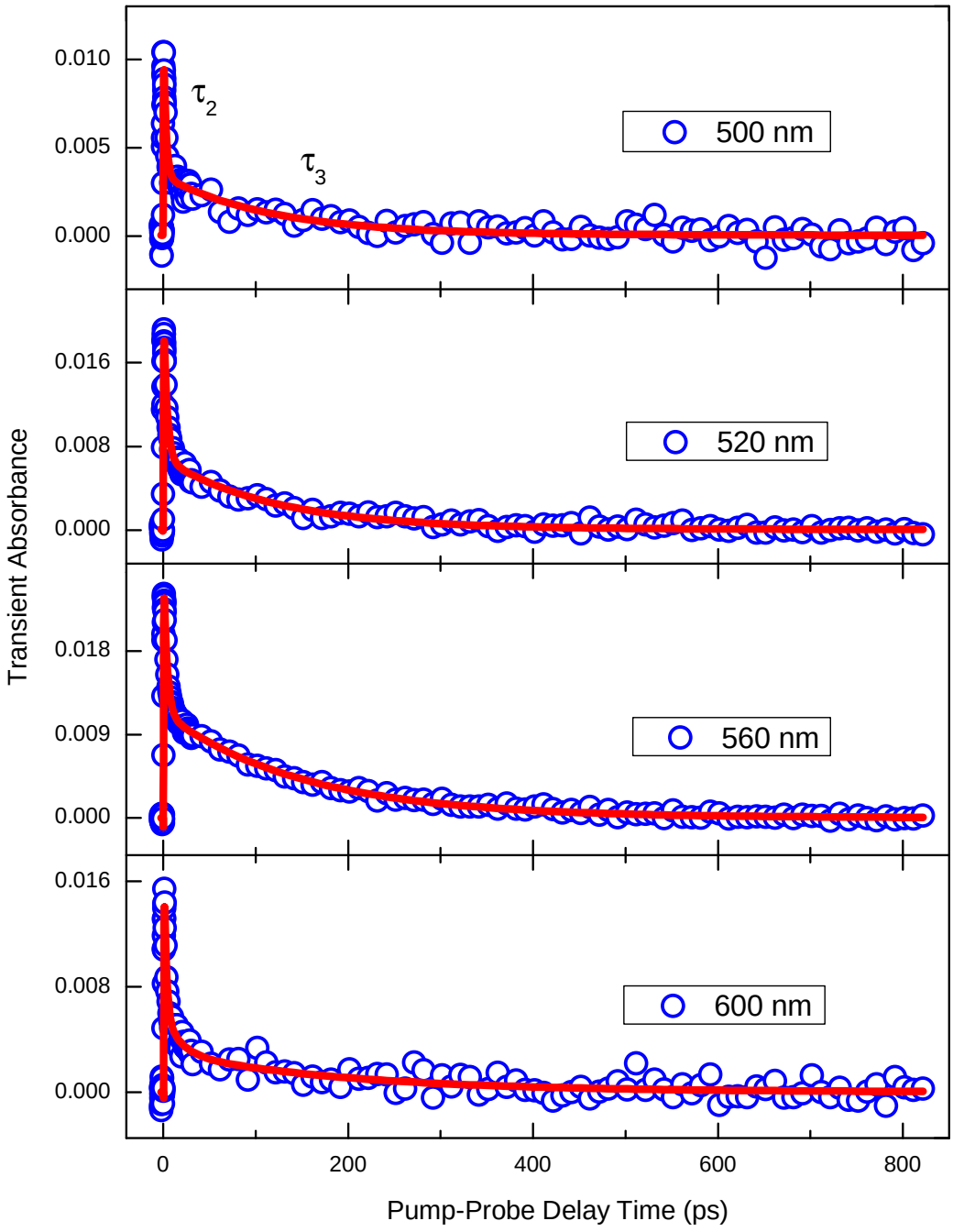

Figure 3.10: Femtosecond time-resolved transient absorption decay kinetic traces of 30 μM ICG in water at four different wavelengths (i.e. 500 nm, 520 nm, 560 nm, and 600 nm). The pump wavelength was 800 nm with an energy of 200 nJ and the probe pulse was white light continuum. The solid line is the best fit to the experimental data.

At all wavelengths measured, the traces showed two distinct decay components suggesting the coexistence of two transient species. The best fits to the experimental data always gave a single rising lifetime of 276 ± 61 fs, and two decay lifetimes of 3.35 ± 0.56 ps and 132 ± 16 ps, respectively. The results of the fitting were summarized into Table 3.1.

Table 3.1: The results of the best fits to the transient absorption decay kinetic traces at four different probe wavelengths: τ_1 is the rising lifetime; τ_2 and τ_3 are the decay lifetimes; A_1, A_2, and A_3 are the pre-exponential factors, respectively.

λ_{probe} (nm)	A_1	A_2	A_3	τ_1 (fs)	τ_2 (ps)	τ_3 (ps)	A_2/A_3
500	-0.012	0.010	0.003	336±61	2.53±0.56	117±16	3.33
520	-0.029	0.016	0.007	309±61	3.66±0.56	120±16	2.29
560	-0.045	0.016	0.011	196±61	3.77±0.56	150±16	1.45
600	-0.026	0.014	0.004	263±61	3.45±0.56	140±16	3.50
Average	–	–	–	276±61	3.35±0.56	132±16	–

The rising lifetime of 276 ± 61 fs corresponds to the formation time of the excited states. The long decay lifetime of 132 ± 16 ps is consistent with the lifetime of $^1ICG^*$ obtained in the previous experiments. We have attributed the short decay lifetime of 3.35 ± 0.56 ps to the lifetime of $[ICG^*]_m$:$[O_2]_n$. This assignment is also supported by the similar observation that the ICG/CDDP complexes have a short decay lifetime of $\sim$5 ps [99]. Moreover, we have found that the two transient species contribute differently to the absorption spectra by calculating the ratios of the pre-exponential factor A_2 to A_3 at different wavelengths. As shown in the last column of Table 3.1, a minimum of the value at 560 nm indicates a more significant contribution from $^1ICG^*$ at this wavelength than the other wavelengths. This is illustrated more clearly in the plot of the pre-exponential factors against the probe wavelength (Figure 3.11). The absorption of $^1ICG^*$ shows a peak at 560 nm, which agrees well with the reported value [68, 100], while that of $[ICG^*]_m$:$[O_2]_n$ exhibits a much broader band with a blue-shifted absorption maximum at around 540 nm.

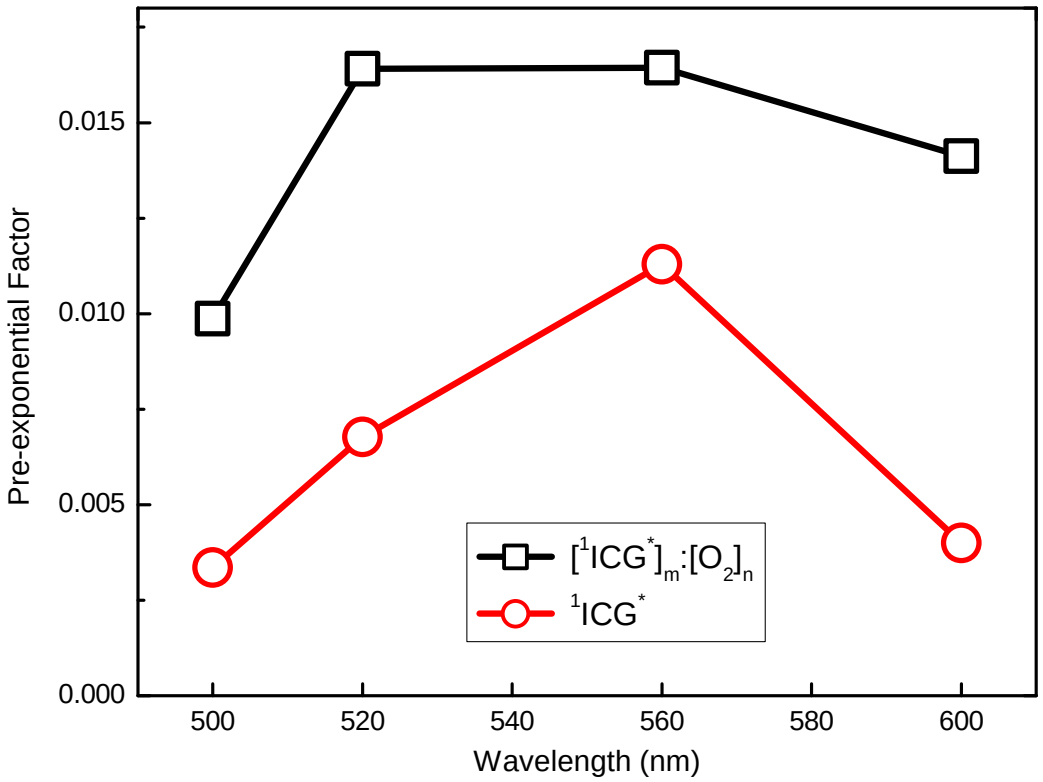

Figure 3.11: The plot of the pre-exponential factors, obtained from the multi-exponential fit of the transient absorption traces, against the probe wavelength.

3.8 Proposed Reaction Mechanism

Basing on all these observations, we have proposed the following reaction pathway:

$$\mathrm{ICG} + \mathrm{O_2} \rightarrow [\mathrm{ICG}]_\mathrm{m} : [\mathrm{O_2}]_\mathrm{n};$$

$$[\mathrm{ICG}]_\mathrm{m} : [\mathrm{O_2}]_\mathrm{n} + \mathrm{h}\nu \rightarrow [\mathrm{ICG}]^*_\mathrm{m} : [\mathrm{O_2}];$$

$$[\mathrm{ICG}]^*_\mathrm{m} : [\mathrm{O_2}] \rightarrow \mathrm{ICG}^{+\bullet} + \mathrm{O_2}^{-\bullet}.$$

The first step is the formation of ICG and oxygen complexes in their ground states. Although this is a rather slow process, once formed, these complexes can dissociate rapidly upon photo-excitation to generate highly reactive species that can cause severe damages to the cancerous tissues.

The Rehm-Weller equation [101] is widely used for calculating the free energy changes associated with photo-induced electron transfer (PET) reactions. It can be written as

$$\Delta\mathrm{G(eV)} = \mathrm{nF}[\mathrm{E_{ox}} - \mathrm{E_{red}}] - \mathrm{w_p} - \mathrm{E_{00}}, \tag{3.4}$$

where n is the number of electrons transferred, F is the Faraday's constant, $\mathrm{E_{ox}}$ is the oxidation potential of the donor, $\mathrm{E_{red}}$ is the reduction potential of the accepter, $\mathrm{w_p}$ describes the coulombic attraction between ions generated by electron transfer, and $\mathrm{E_{00}}$ is the energy of the excited sate. For most electron transfer reactions, nF is approximately equal to one and can be disregarded in the calculations. The work term, $\mathrm{w_p}$, is not applicable to cases where electron transfer occurs between a charged and neutral species, due to the lack of electrostatic attraction between the species, and can therefore be disregarded.

The oxidation potential of ICG in water is 0.76 eV vs Ag/AgCl [89]. The reduction potential for $\mathrm{O_2/O_2^-}$ in water is -0.53 eV vs Ag/AgCl (-0.33 eV vs NHE [102]). With an excitation energy of $\mathrm{E_{00}} = 1.55$ eV, the free energy change of the electron transfer from ICG^* to $\mathrm{O_2}$ can be estimated by using equation 3.4:

$$\Delta\mathrm{G(eV)} = [0.76 - (-0.53)] - 1.55 = -0.26 \text{ eV } (-6.00 \text{ kcal/mol}) < 0.$$

Therefore, the electron transfer reaction between ICG^* and $\mathrm{O_2}$ is energy favorable.

In principle, the transient species (i.e. $ICG^{+\bullet}$ and $O_2^{-\bullet}$) produced by the electron transfer reaction between ICG and O_2 can be detected according to their absorption properties.

Detection of ICG cation radical: Sudeep *et al.* have obtained the transient absorption spectra of ICG cation generated by the radiolysis of O_2 saturated solution in methylene chloride [68]. The dye cation exhibits a broadband in the visible region. However, the absorption band of $ICG^{+\bullet}$ overlaps with that of ICG^*. Thus it is difficult to separate these two species. Moreover, the electron back transfer reaction might have reduced the lifetime of $ICG^{+\bullet}$ to be on the scale of the lifetime of ICG^* [68]. This effect makes the work of identifying $ICG^{+\bullet}$ even more challenging.

Detection of superoxide anion radical: Superoxide anion has an absorption band in the UV range with an absorption maximum at around 240 nm [103]. However, ICG also has strong absorption in this region (Figure 1.5). When using a 266 nm pulse as the probe, we obtained a transient absorption curve similar to Figure 3.4 showing the strong absorption from the ground state of ICG. Therefore, for the detection of $O_2^{-\bullet}$, a proper probe wavelength has to be chosen in order to minimize the contribution from ICG. This is extremely difficult since the molar extinction coefficient of ICG is one order of magnitude larger than that of the superoxide anion. Another problem is that the intensity of our WLC in the UV range is far too weak to be used as the probe for transient absorption spectra measurement. We are seeking other ways to generate continuous UV probe.

Chapter 4

Conclusions

We have performed high-sensitivity time-resolved femtosecond laser spectroscopic experiments on indocyanine green (ICG), which is a potential near infrared (NIR) photosensitizing drug for photodynamic therapy (PDT) applications. For the first time, we studied the initial photochemical reactions leading to the generation of reactive oxygen species (ROS) by using our femtosecond time-resolved laser spectroscopy.

We have obtained the femotosecond time-resolved fluorescence decay kinetic traces of ICG in aqueous solution by applying fluorescence up-conversion technique. The lifetime of the excited singlet state of ICG has been determined to be about 150 ps directly from the fluorescence decay profiles.

The results of the ground state bleaching recovery experiment indicate that ICG has an extremely low yield of excited triplet state ($\Phi_{^3ICG^*} < 0.6\%$) in water. Thus, it is unlikely that large amount of ROS could be generated from the excited triplet state of ICG. This finding is contrary to the conventional understanding that major pathway for ROS generation is the long-lived excited triplet state of the photosensitizers reacting with oxygen molecule. Therefore, there may exist a new reaction pathway for the generation of the ROS, which does not involves the long-lived excited triplet state of drugs.

The results of further studies show that the formation of ICG and oxygen ground-state complexes ($[ICG]_m$:$[O_2]_n$) is a key step in the generation of ROS. Although the formation of this complex is a slow process, the complex can dissociate rapidly, with a lifetime of

about 3.35 ps, upon photoexcitation to produce highly reactive species that can cause tissue damages. A possible reaction pathway is the electron transfer from the excited state of ICG to ground state oxygen, since this reaction has been found to be exothermic from free energy change calculation. In principle, the products of the electron transfer reaction can be detected at proper probe wavelengths. However, the strong and broadband absorption of ICG ground state makes this extremely difficult and additional research will need to be done.

References

[1] R. Ackroyd, C. Kelty, N. Brown, and M. Reed, "The History of Photodetection and Photodynamic Therapy", *Photochem. Photobiol.*, **74**(2001), 656–669. 1

[2] M. R. Detty, S. L. Gibson, and S. J. Wagner, "Current Clinical and Preclinical Photosensitizers for Use in Photodynamic Therapy", *J. Med. Chem.*, **47** (2004), 3897–3915. 1

[3] T. J. Dougherty, G. B. Grindey, R. Fiel, K. R. Weishaupt, and D. G. Boyle, "Photoradiation Therapy. II. Cure of Animal Tumors with Hematoporphyrin and Light", *J. Natl. Cancer Inst.*, **55** (1975), 115–121. 1, 5

[4] Y. Hayata, H. Kato, C. Konaka, J. Ono, and N. Takizawa,"Hematoporphyrin Derivative and Laser Photoradiation in the Treatment of Lung Cancer", *Chest*, **81** (1982), 269–277. 1, 21

[5] D. A. Cortese and J. H. Kinsey, "Hematoporphyrin Derivative Phototherapy in the Treatment of Bronchogenic Carcinoma", *Chest*, **86** (1984), 8–13. 1

[6] E. R. Laws, D. A. Cortese, J. H. Kinsey, R. T. Eagan, and R. E. Anderson, "Photoradiation Therapy in the Treatment of Malignant Brain Tumors: Phase I (feasibility) Study", *Neurosurgery*, **9** (1981), 672–678. 1

[7] J. S. Hill, A. H. Kaye, W. H. Sawyer, G. Morstyn, P. D. Megison, and S. S. Stylli, "Selective Uptake of Hematoporphyrin Derivative into Human Cerebral Glioma", *Neurosurgery*, **26** (1990), 248–254. 1

[8] V. G. Schweitzer, "Photodynamic Therapy for Treatment of Head and Neck Cancer", *Otolaryngol. Head Neck Surg.*, **102** (1990), 225–232. 1

[9] B. L. Wenig, D. M. Kurtzman, L. I. Grossweiner, M. F. Mafee, D. M. Harris, R. V. Lobraico, R. A. Prycz, and E. L. Appelbaum, "Photodynamic Therapy in the Treatment of Squamous Cell Carcinoma of the Head and Neck", *Arch. Otolaryngol. Head Neck Surg.*, **116** (1990), 1267–1270. 1

[10] H. Barr, N. Krasner, P. B. Boulos, P. Chatlani, and S. G. Bown, "Photodynamic Therapy for Colorectal Cancer: a Quantitative Pilot Study", *Br. J. Surg.*, **77** (1990), 93–96. 1

[11] P. N. Prasad, *Introduction to Biophotonics* (John Wiley & Sons, 2003), pp. 433–461. 1, 6, 8, 21, 22

[12] J. Eichler, J. Knof, and H. Lenz, "Measurements on the Depth of Penetration of Light (0.35-1.0 μm) in Tissue", *Radiat. Environ. Biophys.*, **14** (1977), 239–242. 2, 11, 13, 22

[13] L. Foulds, "The Experimental Study of Tumor Progression: a Review", *Cancer Res.*, **14** (1954), 327–339. 2

[14] D. Ford, D. F. Easton, M. Stratton, S. Narod, D. Goldgar, P. Devilee, D. T. Bishop, B. Weber, G. Lenoir, J. Chang-Claude, H. Sobol, M. D. Teare, J. Struewing, A. Arason, S. Scherneck, J. Peto, T. R. Rebbeck, P. Tonin, S. Neuhausen, R. Barkardottir, J. Eyfjord, H. Lynch, B. A. J. Ponder, S. A. Gayther, J. M. Birch, A. Lindblom, D. Stoppa-Lyonnet, Y. Bignon, A. Borg, U. Hamann, N. Haites, R. J. Scott, C. M. Maugard, H. Vasen, S. Seitz, L. A. Cannon-Albright, A. Schofield, M. Zelada-Hedman, and Breast Cancer Linkage Consortium, "Genetic Heterogeneity and Penetrance Analysis of the BRCA1 and BRCA2 Genes in Breast Cancer Families", *Am. J. Hum. Genet.*, **62** (1998), 676–689. 2

[15] E. Warner, W. Foulkes, P. Goodwin, W. Meschino, J. Blondal, C. Paterson, H. Ozcelik, P. Goss, D. Allingham-Hawkins, N. Hamel, L. D. Prospero, V. Contiga, C. Serruya, M. Klein, R. Moslehi, J. Honeyford, A. Liede, G. Glendon, J.-S. Brunet, S. Narod, "Prevalence and Penetrance of BRCA1 and BRCA2 Gene Mutations in Unselected Ashkenazi Jewish Women with Breast Cancer", *J. Natl. Cancer Inst.*, **91** (1999), 1241–1247. 2

[16] H. Risch, J. McLaughlin, D. Cole, B. Rosen, L. Bradley, E. Kwan, E. Jack, D. Vesprini, G. Kuperstein, J. Abrahamson, "Prevalence and Penetrance of Germline BRCA1 and BRCA2 Mutations in a Population Series of 649 Women with Ovarian Cancer", *Am. J. Hum. Genet.*, **68** (2001), 700–710. 2

[17] H. T. Lynch, T. Smyrk, and J. Lynch, "An Update of HNPCC (Lynch Syndrome)", *Cancer Genet. Cytogenet.*, **93** (1997), 84–99. 3

[18] Jr. A. G. Knudson, "Mutation and Cancer: Statistical Study of Retinoblastoma", *Proc. Natl. Acad. Sci.*, **68** (1971), 820–823. 3

[19] Z. Döbrönte, T. Wittmann, and G. Karácsony, "Rapid Development of Malignant Metastases in the Abdominal Wall after Laparoscopy", *Endoscopy*, **10** (1978), 127–130. 3

[20] A. D. Stockdale and T. J. Pocock, "Abdominal Wall Metastasis Following Laparoscopy: a Case Report", *Eur. J. Surg. Oncol.*, **11** (1985), 373–375. 3

[21] L. H. Gray, A. D. Conger, M. Ebert, S. Hornsey, and O. C. Scott, "Concentration of Oxygen Dissolved in Tissues at the Time of Irradiation as a Factor in Radiotherapy", *Br. J. Radiol.*, **26** (1953), 638–648. 4

[22] M. Dean, T. Fojo, and S. Bates, "Tumour Stem Cells and Drug Resistance", *Nat. Rev. Cancer*, **5** (2005), 275–284. 5

[23] G. M. Cooper, *The Cancer Book: A Guide to Understanding the Causes, Prevention, and Treatment of Cancer* (Jones & Bartlett Publishers, 1993), pp. 127–144. 5

[24] D. J. Slamon, B. Leyland-Jones, S. Shak, H. Fuchs, V. Paton, A. Bajamonde, T. Fleming, W. Eiermann, J. Wolter, M. Pegram, J. Baselga, and L. Norton, "Use of Chemotherapy Plus a Monoclonal Antibody Against HER2 for Metastatic Breast Cancer that Overexpresses HER2", *N. Engl. J. Med.*, **344** (2001), 783–792. 5

[25] L. S. Rosen, "VEGF-Targeted Therapy: Therapeutic Potential and Recent Advances", *Oncologist*, **10** (2005), 382–391. 5

[26] J. S. Ross, D. P. Schenkein, R. Pietrusko, M. Rolfe, G. P. Linette, J. Stec, N. E. Stagliano, G. S. Ginsburg, W. F. Symmans, L. Pusztai, and G. N. Hortobagyi, "Targeted Therapies for Cancer 2004", *Am. J. Clin. Pathol.*, **122** (2004), 598–609. 5

[27] D. Murdoch and J. Sager, "Will Targeted Therapy Hold its Promise? An Evidence-Based Review", *Curr. Opin. Oncol.*, **20** (2008), 104–111. 5

[28] O. Raab, "Uber die Wirkung Fluoreszierender Stoffe auf Infusorien", *Z. Biol.*, **39** (1900), 524–546. 5

[29] H. von Tappeiner and A. Jesionek, "Therapeutische Versuche Mit Fluoreszierenden Stoffen", *Muench. Med. Wochenschr*, **47** (1903), 2042–2044. 5, 11

[30] I. Diamond, S. Granelli, A. F. McDonagh, S. Nielsen, C. B. Wilson, and R. Jaenicke, "Photodynamic Therapy of Malignant Tumors", *Lancet*, **2** (1972), 1175–1177. 5

[31] J. F. Kelly, M. E. Snell, and M. C. Berenbaum, "Photodynamic Destruction of Human Bladder Carcinoma", *Br. J. Cancer*, **31** (1975), 237–244. 6, 21

[32] T. J. Dougherty, J. E. Kaufman, A. Goldfarb, K. R. Weishaupt, D. Boyle, and A. Mittleman, "Photoradiation Therapy for the Treatment of Malignant Tumors", *Cancer Res.*, **38** (1978), 2628–2635. 6, 12, 21

[33] T. Vo-Dinh, *Biomedical Photonics Handbook* (CRC Press, 2003), pp.28–4. 6

[34] W. M. Sharman, C. M. Allen, and J. E. van Lier, "Role of Activated Oxygen Species in Photodynamic Therapy", *Methods Enzymol.*, **319** (2000), 376–400. 6

[35] C. S. Foote, "Definition of Type I and Type II Photosensitized Oxidation", *Photochem. Photobiol.*, **54** (1991), 659.

[36] M. Ochsner, "Photophysical and Photobiological Processes in the Photodynamic Therapy of Tumors", *J. Photochem. Photobiol. B: Biol.*, **39** (1997), 1–18. 6

[37] T. J. Dougherty, C. J. Gomer, B. W. Henderson, G. Jori, D. Kessel, M. Korbelik, J. Moan, and Q. Peng, "Photodynamic Therapy", *J. Natl. Cancer Inst.*, **90** (1998), 889–905. 8

[38] D. E. Dolmans, D. Fukumura, and R. K. Jain, "Photodynamic Therapy for Cancer", *Nat. Rev. Cancer*, **3** (2003), 380–387. 8, 13

[39] N. I. Krinsky, "Singlet Excited Oxygen as a Mediator of the Antibacterial Action of Leukocytes", *Science*, **186** (1974), 363–365. 8

[40] K. R. Weishaupt, C. J. Gomer, and T. J. Dougherty, "Identification of Singlet Oxygen as the Cytotoxic Agent in Photo-inactivation of a Murine Tumor", *Cancer Res.*, **36** (1976), 2326–2329. 8

[41] G. Herzberg, *Spectra of Diatomic Molecules* (van Nostrand, 1951). 9

[42] A. P. Schaap, *Singlet Moelcular Oxygen* (John Wiley & Sons, 1976). 9

[43] D. Kessel, "Effects of Photoactivated Porphyrins at the Cell Surface of Leukemia L1210 Cells", *Biochemistry*, **16** (1977), 3443–3449. 10

[44] Z. Malik and M. Djaldetti, "Destruction of Erythroleukemia, Myelocytic Leukemia and Burkitt Lymphoma Cells by Photoactivated Protoporphyrin", *Int. J. Cancer*, **26** (1980), 495–500.

[45] D. A. Bellnier and T. J. Dougherty, "Membrane Lysis in Chinese Hamster Ovary Cells Treated with Hematoporphyrin Derivative Plus Light", *Photochem. Photobiol.*, **36** (1982), 43–47.

[46] D. Kessel, "Hematoporphyrin and HpD: Photophysics, Photochemistry and Phototherapy", *Photochem. Photobiol.*, **39** (1984), 851–859. 10

[47] D. P. Valenzeno, "Photomodification of Biological Membranes with Emphasis on Singlet Oxygen Mechanisms", *Photochem. Photobiol.*, **46** (1987), 147–160. 10

[48] W. Korytowski and A. W. Girotti, "Singlet Oxygen Adducts of Cholesterol: Photogeneration and Reductive Turnover in Membrane Systems", *Photochem. Photobiol.*, **70** (1999), 484–489. 10

[49] F. Wilkinson, W. P. Helman, and A. B. Ross, "Quantum Yields for the Photosensitized Formation of the Lowest Electronically Excited Singlet State of Molecular Oxygen in Solution", *J. Phys. Chem. Ref. Data*, **22** (1993), 113–150. 10

[50] J. G. Parker and W. D. Stanbro, "Optical Determination of the Rates of Formation and Decay of $^1O_2$ in H_2O, D_2O and Other Solvents", *J. Photochem.*, **25** (1984), 545–547. 10

[51] J. Prime, *Les Accidentes Toxiques Par L'eosinate de Sodium* (Jouve adn Boyer, 1900). 11

[52] I. J. Macdonald and T. J. Dougherty, "Basic Principles of Photodynamic Therapy", *J. Porphryins Phthalocyanines*, **5** (2001), 105–129. 12

[53] M. Triesscheijin, P. Baas, J. H. M. Schellens, and F. A. Stewart, "Photodynamic Therapy in Oncology", *The Oncologist.*, **11** (2006), 1034–1044. 13

[54] P. Taroni, A. Pifferi, A. Torricelli, D. Comelli, and R. Cubeddu, "*In vivo* Absorption and Scattering Spectroscopy of Biological Tissues", *Photochem. Photobiol. Sci.*, **2** (2003), 124–129. 13, 14

[55] E. C. Bradley and J. W. Barr, "Determination of Blood Volume Using Indocyanine Green (Cardio-Green®) Dye", *Life Sci.*, **7** (1968), 1001–1007. 13, 23

[56] A. Craandijk and C. A. van Beek, "Indocyanine Green Fluorescence Angiography of the Choroid", *Br. J. Oppthalmol.*, **60** (1976), 377–385. 13

[57] R. W. Flower and B. F. Hochheimer, "Indocyanine Green Dye Fluorescence and Infrared Absorption Choroidal Angiography Performed Simultaneously with Fluorescein Angiography", *Johns. Hopkins. Med. J.*, **138** (1976), 33–42. 13

[58] K. Haneda and T. Horiuchi, "A Method for Measurement of Total Circulating Blood Volume Using Indocyanine Green", *Tohoku J. Exp. Med.*, **148** (1986), 49–56. 13

[59] K. Sauda, T. Imasaka, and N. Ishibashi, "Determination of Protein in Human Serum by High-Performance Liquid Chromatography with Seimconductor Laser Fluorometric Detection", *Anal. Chem.*, **58** (1986), 2649–2653. 13

[60] J. C. Fleishaker, H. Friedman, and S. R. Pollock, "Extent and Variability of the First-Pass Elimination of Adinazolam Mesylate in Health Male Volunteers", *Pharm. Res.*, **8** (1991), 162–167. 13, 23

[61] M. L. J. Landsman, G. Kwant, G. A. Mook, and W. G. Zijlstra, "Light-Absorbing Properties, Stability, and Spectral Stabilization of Indocyanine Green", *J. Appl. Physiol.*, **40** (1976), 575–583. 13, 23, 32, 34

[62] Y. Gu, J.-H. Li, and Z.-H. Gou, "Selective Protection of Normal Hepatocytes by Indocyanine Green in Photodynamic Therapy for the Hepatoma of Rat", *Proc. SPIE*, **1616** (1991), 266–274. 13

[63] S. Fickweiler, R.-M. Szeimies, W. Bäumler, P Steinbach, S. Karrer, A. E. Goetz, C. Abels, and F. Hofstädterb, "Indocyanine Green: Intracellular Uptake and Phototherapeutic Effects *in Vitro*", *J. Photochem. Photobiol. B: Biol.*, **38** (1997), 178–183. 13, 22

[64] C. Abels, S. Karrer, W. Bäumler, A. E. Goetz, M. Landthaler, and R. M. Szeimies, "Indocyanine Green and Laser light for the Treatment of AIDS-Associated Cutaneous Kaposi's Sarcoma", *Br. J. Cancer*, **77** (1998), 1021–1024.

[65] W. Bäumler *et al.*, C. Abels, S. Karrer S, T. Weiss, H. Messmann, M. Landthaler, and R.-M. Szeimies, "Photo-oxidative Killing of Human Colonic Cancer Cells Using Indocyanine Green and Infrared Light", *Br. J. Cancer*, **80** (1999), 360–363. 13, 22

[66] E. Engel, R. Schraml, T. Maisch, K. Kobuch, B. König, R.-M. Szeimies, J. Hillenkamp, W. Bäumler, and R. Vasold, "Light-Induced Decomposition of Indocyanine Green", *Invest. Ophthalmol. Vis. Sci.*, **49** (2008), 1777–1783. 15

[67] H. Gratz, A. Penzkofer, C. Abels, R.-M. Szeimies, M. Landthaler, and W. Bäumler, "Photo-Isomerisation, Triplet Formation, and Photo-Degradation Dynamics of Indocyanine Green Solutions", *J. Phtochem. Photobiol. A: Chem.*, **128** (1999), 101–109. 15, 22, 31

[68] P. K. Sudeep, K. Takechi, and P. V. Kamat, "Harvesting Photons in the Infrared. Electron Injection from Excited Tricarbocyanine Dye (IR-125) into TiO2 and Ag@TiO2 Core-Shell Nanoparticles", *J. Phys. Chem. C*, **111** (2007), 488–494. 15, 22, 28, 31, 41, 44

[69] A. H. Zewail, "Femtochemistry: Atomic-Scale Dynamics of the Chemical Bond Using Ultrafast Lasers (*Noble Lecture*)", *Angew. Chem. Int. Ed.*, **39** (2000), 2586–2631. 17, 32

[70] J. Shah, "Ultrafast Luminescence Spectroscopy Using Sume Frequency Generation", *IEEE Journal of Quantum Electronics*, **24** (1988), 276–288. 18

[71] H. E. Lessing and A. von Jena, "Separation of Rotational Diffusion and Level Kinetics in Transient Absorption Spectroscopy", *Chem. Phys. Lett.*, **42** (1976), 213–217. 20

[72] H. Silver, "Psoriasis Vulgaris Treated with Hematoporphyrin", *Arch. Dermatol. Syphilol.*, **36** (1937), 1118–1119. 21

[73] J. W. Miller, U. Schmidt-Erfurth, M. Sickenberg, C. J. Pournaras, H. Laqua, I. Barbazetto, L. Zografos, B. Piguet, G. Donati, A.-M. Lane, R. Birngruber, H. van den Berg, H. A. Strong, U. Manjuris, T. Gray, M. Fsadni, N. M. Bressler, and E. S. Gragoudas, "Photodynamic Therapy with Verteporfin for Choroidal Neovascularization Caused by Age-related Macular Degeneration: Results of a Single Treatment in a Phase 1 and Phase 2 Study", *Arch. Ophthalmol.*, **117** (1999), 1161–1173. 21

[74] U. Schmidt-Erfurth, J. W. Miller, M. Sickenberg, H. Laqua, I. Barbazetto, E. S. Gragoudas, L. Zografos, B. Piguet, C. J. Pournaras, G. Donati, A.-M. Lane, R. Birngruber, H. van den Berg, H. Strong, U. Manjuris, T. Gray, M. Fsadni, and N. M. Bressler, "Photodynamic Therapy with Verteporfin for Choroidal Neovascularization Caused by Age-related Macular Degeneration: Results of Retreatment in a Phase 1 and Phase 2 Study", *Arch. Ophthalmol.*, **117** (1999), 1177–1187. 21

[75] S. B. Brown, E. A. Brown, and I. Walker, "The Present and Future Role of Photodynamic Therapy in Cancer Treatment", *Lancet. Oncol.*, **5** (2004), 497–508. 21

[76] D. F. O'Brien, T. M. Kelly, and L. F. Costa, "Excited State Properties of Some Carbocyanine Dyes and the Energy Transfer Mechanism of Spectral Sensitization", *Photogr. Sci. Eng.*, **18** (1974), 76–84. 22, 31

[77] D. M. Sturmer, *Kirk-Othmer Encyclopedia of Chemical Technology* (John Wiley & Sons, Inc., 2004). 22

[78] S. Reindl, A. Penzkofer, S.-H. Gong, M. Landthaler, R. M. Szeimies, C. Abels, and W. Bäumler, "Quantum Yield of Triplet Formation for Indocyanine Green", *J. Phtochem. Photobiol. A: Chem.*, **105** (1997), 65–68. 22, 31

[79] S. A. Soper and Q. L. Mattingly, "Steady-State and Picosecond Laser Fluorescence Studies of Nonradiative Pathways in Tricarbocyanine Dyes: Implications to the Design of Near-IR Fluorochromes with High Fluorescence Efficiencies", *J. Am. Chem. Soc.*, **116** (1994), 3744–3752. 22, 26, 28

[80] I. J. Fox, L. G. S. Brooker, D. W. Heseltine, H. E. Essex, and E. H. Wood, "New Dyes for Continuous Recording of Dilution Curves in Whole Blood Independent of Variations in Blood Oxygen Saturation (Abstr.)", *Am. J. Physiol.*, **137** (1956), 599. 23

[81] G. Moneta, M. Brülisauer, K. Jäger, and A. Bollinger, "Infrared Fluorescence Videomicroscopy of Skin Capillaries with Indocyanine Green", *Int. J. Microcirc. Clin. Exp.*, **6** (1987), 25–34. 23

[82] J. Gathje, R. R. Steuer, and K. R. K. Nicholes, "Stability Studies on Indocyanine Green Dye", *J. Appl. Physiol.*, **29** (1970), 181–185. 23, 32

[83] R. Simmons and R. J. Shephard, "Does Indocyanine Green Obey Beer's Law?", *J. Appl. Physiol.*, **30** (1971), 502–507. 24

[84] O. G. Björnsson, R. Murphy, and V. S. Chadwick, "Physicochemical Studies of Indocyanine Green (ICG): Absorbance/Concentration Relationship, pH Tolerance and Assay Precision in Various Solvents", *Cell. Mol. Life Sci.*, **38** (1982), 1441–1442.

[85] J. F. Zhou, M. P. Chin, and S. A. Schafer, "Aggregation and Degradation of Indocyanine Green", *Proc. SPIE*, **2128** (1994), 495–505.

[86] F. Rotermund, R. Weigand, and A. Penzkoer, "J-aggregation and Disaggregation of Indocyanine Green in Water", *Chemical Physics*, **220** (1997), 385–392.

[87] W. Holzer, M. Mauerer, A. Penzkofer, R.-M. Szeimies, C. Abels, M. Landthaler, and W. Bäumler, "Photostability and Thermal Stability of Indocyanine Green", *J. Photochem. Photobiol. B: Biol.*, **47** (1998), 155–164. 23

[88] R. Philip, A. Penzkofer, W. Bäumler, R. M. Szeimies, and C. Abels, "Absorption and Fluorescence Spectroscopic Investigation of Indocyanine Green", *J. Photochem. Photobiol. A: Chem.*, **96** (1996), 137–148. 24, 26, 28, 31, 34

[89] S. K. Lee and A. J. Bard, "Near-Ir Electrogenerated Chemiluminescence of Tricarbocyanine Dyes in Micellar Systems", *Anal. Lett.*, **31** (1998), 2209–2229. 24, 43

[90] A. R. Horrocks, T. Medinger, and F. Wilkinson, "A New Accurate Method for Determining the Quantum Yields of Triplet State Production of Aromatic Molecules in Solution", *Chem. Commun.*, (1965), 452. 28

[91] A. A. Lamola and G. S. Hammond, "Mechanisms of Photochemical Reactions in Solution. XXXIII. Intersystem Crossing Efficiencies", *J. Chem. Phys.*, **43** (1965), 2129–2135. 28

[92] C. A. Parker and T. A. Joyce, "Triplet Formation Efficiencies from Delayed Fluorescence Measurements", *Chem. Commun.*, (1966), 234–235. 28

[93] J. S. Bruinen, "Application of Electron Spin Resonance in the Study of Triplet States. III. Extinction Coefficients of Triplet-Triplet Transitions", *J. Chem. Phys.*, **49** (1968), 586–590. 28

[94] R. Bensasson, C. R. Goldschmidt, E. J. Land, and T. G. Truscott, "Laser Intensity and the Comparative Method for Determination of Triplet Quantum Yields", *Photochem. Photobiol.*, **28** (1978), 277–281. 28

[95] S. Nonell, P. F. Aramendia, K. Heihoff, R. M. Negri, and S. E. Braslavsky, "Laser-Induced Optoacoustics Combined with Near-Infrared Emission. An Alternative Approach for the Determination of Intersystem Crossing Quantum Yields Applied to Porphycenes", *J. Phys. Chem.*, **94** (1990), 5879–5883. 28

[96] B. Lament, J. Karpiuk, and J. Waluk, "Determination of Triplet Formation Efficiency from Kinetic Profiles of the Ground State Recovery", *Photochem. Photobiol. Sci.*, **2** (2003), 267–272. 28

[97] S. Reindl and A. Penzkofer, "Triplet Quantum Yield Determination by Picosecond Laser Double-Pulse Fluorescence Excitaion", *Chemical Physics*, **213** (1996), 429–438. 31

[98] C. Haritoglou, W. Freyer, S. G. Priglinger, and A. Kampik, "Light Absorbing Properties of Indocyanine Green (ICG) in Solution and After Absorption to the Retinal

Surface - an ex-vivo Approach", *Graefe's Arch. Clin. Exp. Ophthalmol.*, **244** (2006), 1196–1202. 34

[99] Q.-B. Lu, "Molecular Reaction Mechanisms of Combination Treatments of Low-Dose Cisplatin with Radiotherapy and Photodynamic Therapy", *J. Med. Chem.*, **50** (2007), 2601–2604. 41

[100] Y. H. Meyer, M. Pittman, and P. Plaza, "Transient Absorption of Symmetrical Carbocyanines", *J. Photochem. Photobiol. A: Chem.*, **114** (1998), 1–21. 41

[101] D. Rehm and A. Weller, "Kinetics of Fluorescence Quenching by Electron Transfer and H-atom Transfer", *Isr. J. Chem*, **8** (1970), 259. 43

[102] Y. A. Ilan, G. Czapski, and D. Meisel, "The One-Electron Transfer Redox Potentials of Free Radicals. I. The Oxygen/Superoxide System", *Biochim. Biophys. Acta.*, **430** (1976), 209–224. 43

[103] J. Rabani and S. O. Nielsen, "Absorption Spectrum and Decay Kinetics of O_2^- and HO_2 in Aqueous Solutions by Pulse Radiolysis", *J. Phys. Chem.*, **73** (1969), 3736–3744. 44